Contents lists available at SciOpen

Food Science and Human Wellness

journal homepage: https://www.sciopen.com/journal/2097-0765

China Food Publishing Co.

Laetiporus sulphureus polysaccharides ameliorate chronic alcoholic liver disease by activating p62/Nrf2, AMPK pathways and reshaping gut microbiota

Huajie Zhao[a,*], Liang Liu[a], Ningning Liu[a], Baoguo Deng[a], Min Li[a], Duan Li[a], Le Jia[b], Ge Wang[a,*], Fan Yang[a,*]

[a] *School of Basic Medical Sciences, Xinxiang Medical University, Xinxiang 453003, China*
[b] *College of Life Science, Shandong Agricultural University, Tai'an 271018, China*

ARTICLE INFO

Article history:
Received 17 June 2024
Received in revised form 13 July 2024
Accepted 26 August 2024

Keywords:
Laetiporus sulphureus polysaccharides
Alcoholic liver disease
Lipid metabolism
Oxidative stress
Gut microbiota

ABSTRACT

One novel enzymatic-extractable polysaccharide (ES1) from fruiting bodies of *Laetiporus sulphureus* was obtained by isolation and purification using a DEAE Seplife FF chromatographic column and a Sephacryl S-400HR column. The hepatoprotective ability of ES1 against chronic alcoholic liver disease (ALD) and its underlying mechanism were explored. The results indicated that ES1 could alleviate liver damage in ALD mice by activating sequestosome-1/nuclear factor E2-related factor 2 (P62/Nrf2) pathway to increase antioxidant enzyme activities against oxidative stress, regulating adenosine monophosphate-activated protein kinase (AMPK) pathway to promote fatty acid oxidation and inhibit cholesterol synthesis against lipid metabolism disorders, and improving gut microbiota (increasing the relative abundances of *Ligilactobacillus* and *Akkermansia*, and reducing the relative abundances of *Enterococcus*, *Romboutsia*, *Allobaculum*, Coriobacteriaceae_UCG-002, *Dubosiella* and *Faecalibaculum*) against intestinal barrier dysfunction. Meantime, structural analysis showed that ES1 with molecular weight of 25.79 kDa was composed of *α*-*D*-Man*p*-(1→, →2,6)-*α*-*D*-Gal*p*-(1→, →6)-*α*-*D*-Gal*p*-(1→, →3)-*α*-*L*-Fuc*p*-(1→, and *α*-*D*-Glc*p*-(1→, and its structure was also inferred. Therefore, these data support the application of ES1 as a potential functional food or drug for treating ALD.

1. Introduction

Alcoholic liver disease (ALD) is the most common type of chronic liver disease worldwide, manifesting as alcohol-induced hepatitis, cirrhosis, liver fibrosis, fatty liver and so on[1]. ALD, the second-most liver diseases after viral hepatitis, has brought a heavy burden to national economic development and social stability and become an important public health problem[2-3]. At present, the molecular mechanisms of its occurrence and development are not fully understood, and it is generally believed that oxidative stress, lipid metabolism disorders, gut microbiota, immunologic injury and intestinal endotoxemia play an important role in ALD progression[4-5]. Although the research on ALD pathogenesis has made breakthrough progress, the prevention and effective treatment of ALD have not been significantly improved. Until now, the treatment and prevention methods of ALD and its complications are still mainly oral or injection of chemical synthesis drugs, most of which possess harmful adverse side effects. Therefore, there is an urgent need to detect new natural active drugs and potential therapeutic targets against ALD.

A lot of evidence have showed that ALD is closely related to oxidative stress[1,6]. Excessive alcohol consumption can stimulate excessive reactive oxygen species (ROS) production including superoxide, hydroxyl radical and hydrogen peroxide to reduce

* Corresponding author at: School of Basic Medical Sciences, Xinxiang Medical University, Xinxiang 453003, China
Email address: zhaohuajiebest@163.com (H.J. Zhao); 071033@xxmu.edu.cn (G. Wang); yangf77@xxmu.edu.cn (F. Yang)
Peer review under responsibility of Beijing Academy of Food Sciences.

SciOpen Publishing services by Tsinghua University Press

http://doi.org/10.26599/FSHW.2024.9250405

intracellular antioxidant levels for forming oxidative stress, thereby leading to liver damage[7]. Antioxidant enzymes are crucial important part in endogenous antioxidant defense system for clearing ROS and maintaining the balance of redox reaction in cells[8]. Therefore, activating the antioxidant system can promote the elimination of ROS, thereby alleviating ALD[9]. Nuclear factor E2-related factor 2 (Nrf2) is the main regulatory factor of antioxidant enzymes including NAD(P)H quinone oxidoreductase 1 (NQO1) and superoxide dismutase 1 (SOD1) against oxidative stress[10]. Furthermore, p62 protein, a stress sensor coded by sequestosome 1 gene, can competitively bind Keap1, and then bind to the autophagosome membrane to degrade Keap1 for activating Nrf2[6,10]. These reports have showed that p62-Nrf2 signaling pathway, a new therapeutic target, may be a potential treatment for ALD.

Alcohol intake negatively regulates normal lipid metabolism in liver, and the earliest and most common adverse reaction of the liver to alcohol is hepatic steatosis, the severity of which is thought to be closely associated with late progression of ALD. Adenosine monophosphate-activated protein kinase (AMPK), a critical regulator of lipid accumulation in ALD, can restore energy homeostasis by inhibiting liver lipid synthesis and other energy consumption paths[6]. Some reports have displayed that alcohol can cause fat accumulation by inhibiting AMPK signaling pathway[11]. In the process of occurrence and development of ALD, sterol regulatory element binding protein-1c (SREBP-1c) exerts its harmful effects by increasing the biosynthesis of fatty acids, and peroxisome proliferators-activated receptors alpha (PPARα) is a key transcription factor that inhibits triglyceride (TG) accumulation and enhances enzymatic defense against oxidative stress by activating fatty acid oxidation[12]. Hence, activating AMPK signaling pathway is a potential strategy for prevention and treatment against ALD.

Meantime, mounting evidence reveal that the “gut-liver axis” is closely related to the formation of chronic liver disease[13]. Some studies also have verified that gut microbiota and intestinal barrier play a key role in ALD development[14]. Excessive alcohol consumption can cause the overgrowth of Gram-negative bacteria against composition of gut microbiota, thereby affecting its metabolites[15]. These changes can disrupt the intestinal barrier function and the integrity of tight junctions to result in “intestinal leakage” phenomenon and intestinal microbial translocation, thereby causing that gut microbiota and metabolites is transported to liver *via* the portal vein for liver injury[16]. Llopis et al.[17] and Philips et al.[18] have proved that fecal transplant can alleviate alcohol-induced liver damage, indicating that gut microbiota is a potential therapeutic target. Therefore, it is necessary to screen a natural product or drug that can regulate gut microbiota against ALD.

Edible mushroom polysaccharides have a wide variety of biological functions, such as intestinal microbial regulation, antioxidant, anti-cancer, hepatoprotection and so on[19-21], which has become a resource bank of natural medicine. *Laetiporus sulphureus*, a precious wild fungus, has many medicinal properties against cancer, inflammatory, virus and so on[21]. That is because it contains multiple active substances, including triterpenoids, phenolics, polysaccharides and others, and its bioactivities are connected with its polysaccharides[22]. Our previous work has displayed that polysaccharides from spent mushroom substrates (*L. sulphureus*) can improve acute alcohol-induced hepatic injury, especially enzymatic-extractable polysaccharides[23]. However, its underlying mechanisms of enzymatic-extractable polysaccharides from *L. sulphureus* fruiting bodies (ES) against chronic ALD have not been investigated. Therefore, based on the above reasons, we raised the scientific question of whether one novel enzymatic-extractable polysaccharide (ES1, main component isolated from ES) might alleviate chronic ALD by regulating P62/Nrf2 and AMPK pathways and gut microbiota. Meantime, for better application in medicine and food, chemical structure of ES1 was also clarified.

2. Materials and methods

2.1 ES preparation and its purification

The dried and pulverized fruiting bodies of *L. sulphureus* were filtered by 60-mesh sieve. The obtained powder was mixed with 4-fold volumes of ethyl alcohol for eliminating fat-soluble pigments and some impurities, and then the mixture was centrifuged (3 000 r/min, 10 min) to collect precipitate. After the dried precipitate mixed with snailase solutions (4% (*m/V*), 37 °C, 6 h), the supernatant was collected (3 000 r/min, 10 min), concentrated, and then incubated with 4 volumes of ethanol at 4 °C overnight to offer crude polysaccharide extract by centrifugation (3 000 r/min, 10 min). The dissolved crude polysaccharide extract was processed by incubation with Sevag reagent, petroleum ether and microporous resin AB-8, respectively. The reclaimed water phase was dialyzed and lyophilized to obtain the polysaccharides named ES.

ES solution (10 mg/mL), injected into DEAE Seplife FF chromatographic column (26 mm × 400 mm), was eluted with 0, 0.1, 0.2 and 0.3 mol/L NaCl at a flow rate of 4 mL/min, and the eluate (15 mL/tube) was collected. The main fraction (tubes 7−19) was obtained and designed as ES1. To get a purer ES1, ES1 was purified on Sephacryl S-400HR column (26 mm × 1 000 mm) and eluted with deionized water at a flow rate of 0.5 mL/min for 10 min/tube. In this work, tubes 35−49 were collected for follow-up experiment. The molecular weight (*M*w) range for the purification was 1×10^4–2×10^6 Da. Throughout the purification process, each tube was monitored by the phenol-sulfuric acid method. Finally, the single and uniform fraction (ES1) was obtained. The protein content of ES1 was detected by Coomassie brilliant blue method with bovine serum albumin (BSA) as reference material.

2.2 Structural elucidation of ES1

2.2.1 UV-Vis analysis

The UV-Vis spectrum of ES1 was recorded by a Multiskan GO multifunctional enzyme marker over a wavelength range of 200−1 000 nm.

2.2.2 Fourier transform infrared spectroscopy (FT-IR)

The mixture including appropriate ES1 and 200 mg KBr was pressed into thickness of 1 mm sheet, which was detected using a Nicolet iZ-10 FT-IR at the wavelength range of 4 000−400 cm^{-1}.

2.2.3 Mw determination

*M*w was measured using gel permeation chromatography-differential refractive index-multi-angle laser light scattering (GPC-RI-MALSI). ES1, dissolved in $NaNO_3$ solution (0.1 mol/L) containing 0.02% NaN_3 at the concentration of 1 mg/mL, was filtered through a filter of 0.45 μm pore size. The loading quantity, mobile phase and flow rate of ES1 were 100 μL, 0.1 mol/L $NaNO_3$ solution containing 0.02% NaN_3 and 0.4 mL/min, respectively.

2.2.4 Monosaccharide compositions analysis

The monosaccharide composition of ES1 was analyzed using ICS-5000 high performance liquid chromatography (HPLC) system. ES1 and monosaccharide standards were processed by the previous method[24]. Monosaccharide standards were composed of fucose (Fuc), rhamnose (Rha), arabinose (Ara), galactose (Gal), glucose (Glc), xylose (Xyl), mannose (Man), fructose (Fru), ribose (Rib), galacturonic acid (Gal-UA), glucuronic acid (Glc-UA), mannuronic acid (Man-UA) and guluronic acid (Gul-UA).

2.2.5 Glycosyl linkage analysis

The methylation analysis of ES1 was conducted by the previously reported[25]. The processed ES1 by a series of chemical reactions was analyzed by gas chromatography-mass spectrometry (GC-MS).

2.2.6 Nuclear magnetic resonance (NMR) analysis

The ^{1}H NMR, ^{13}C NMR, ^{1}H-^{1}H correlation spectroscopy (COSY), ^{1}H-^{13}C heteronuclear singular quantum correlation (HSQC), ^{1}H-^{13}C heteronuclear multiple bond correlation (HMBC) and ^{1}H-^{1}H nuclear overhauser effect spectroscopy (NOESY) was recorded by Bruker Avance III 600 MHz spectrometer. Before loading, ES1 was dissolved in D_2O at the concentration of 40 mg/mL.

2.3 Hepatoprotective experiments of ES1 against chronic ALD in mice

2.3.1 Animal model and treatment

Animal experiment was performed according to procedures approved by the Institutional Animal Care and Use Committee of Xinxiang Medical University (XYLL-20210279) in accordance with ARRIVE guidelines. C57BL/6 mice (male, 7−8 weeks, 20−22 g, n = 36) were purchased from Henan Skobes Biotechnology Co., Ltd. (SCXK (Yu) 2020-0005), and fed in a specific pathogen-free animal room at (23 ± 1) °C with a relative humidity of (50 ± 5)% under a 12 h light/dark cycle. During the adaptive feeding period, all mice were free access to food and water.

The domesticated mice were randomly divided into 3 groups with 12 mice in each group including normal saline (NS) group, alcohol model (EtOH) group and ES1 treatment (ES) group. The NS group was fed Lieber-DeCarli regular liquid diet without alcohol, whereas the EtOH and ES groups were fed Lieber-DeCarli alcoholic liquid diet. At week 5, the ES group was given ES1 (400 mg/(kg·day)) according to our previous study[23], while the NS and EtOH groups received equal volume of normal saline. The experiment lasted for 12 weeks, and the experimental flow chart was displayed in Fig. 1. During the 12th week, the collected feces from all mice were used for assessing gut microbiota diversity. At the end of the experiment, all mice were anesthetized with sodium pentobarbital after fasting for 12 h, and the blood, liver, colon were collected for further test. The liver index was determined by the following formula:

$$\text{Liver index (\%)} = \frac{\text{Liver weight}}{\text{Body weight}} \times 100 \quad (1)$$

2.3.2 Biochemical parameters analysis

The obtained serum was used for evaluating serum biochemical indicators including alanine aminotransferase (ALT), aspartate transaminase (AST), total cholesterol (TC), TG and high-density lipoprotein cholesterol (HDL-C).

A portion of the collected liver tissue, mixed with pre-cooled PBS in a ratio of 1:9, was ground and centrifuged (3 000 r/min, 10 min, 4 °C). The obtained supernatant was applied for assessing malonaldehyde (MDA), superoxide dismutase (SOD), catalase (CAT) and glutathione peroxidase (GSH-Px).

2.3.3 Hematoxylin-eosin (H&E) and Oil red O staining

The part of the collected liver and colon was soaked in 4% paraformaldehyde. H&E and Oil red O staining was performed according to the previous method[26], and the stained slices were observed and photographed by a microscope.

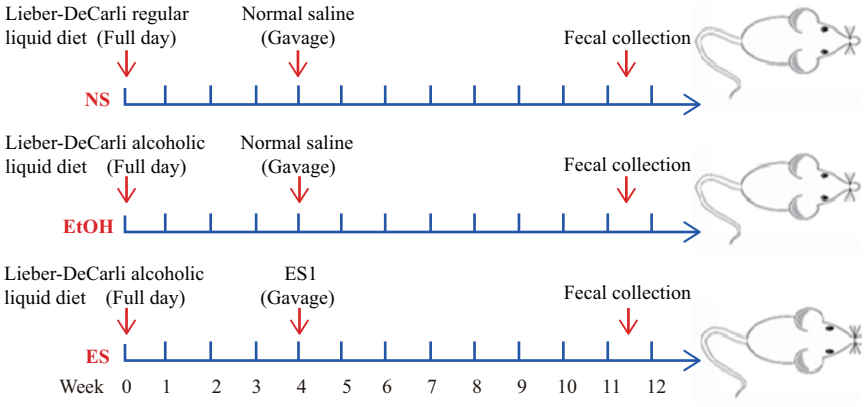

Fig. 1 Flow chart of animal experiment.

2.3.4 ROS test

The frozen livers were sliced into 6 μm sections, while the frozen slices were rewarmed at room temperature, and incubated with ROS staining solution and DAPI. After seal sheet, the stained slice was observed and photographed by fluorescence microscope.

2.3.5 Western blot analysis

All sample were pretreated by the method of our previous study[20]. The processed samples were electrophoresed on a 10% SDS-polyacrylamide gel and transferred to PVDF membranes. After blocked by 5% nonfat-milk for 2 h, the PVDF membranes were incubated with primary antibodies at 4 °C overnight, and the information of primary antibodies was displayed in Table S1. Afterwards, the above PVDF membranes were incubated with the secondary antibodies for 2 h, and the target protein bands processed by chemiluminescent solution were detected by using a chemiluminescence analyzer.

2.3.6 Immunofluorescence analysis

Liver tissue sections were prepared as previous introduced in Section 2.3.3. After dewaxing, permeabilization, antigen reparation and blocking, the tissue sections were incubated with antibody of Nrf2 at 4 ℃ overnight, and at subsequently incubated with cy3-labeled goat anti-rabbit antibody at room temperature for 1 h. After sealed by antifade mounting medium, the stained tissues sections were observed and photographed by fluorescence microscope.

2.3.7 Gut microbiota analysis

Total microbial DNA from feces among three groups were extracted by using TIANamp stool DNA kit by manufacturer's instructions, and DNA concentration and integrity were assessed by a NanoDrop® ND-2000 spectrophotometer and 1.0% agarose gel electrophoresis, respectively. The 16S rRNA sequencing was performed by Majorbio Biotechnology Co., Ltd. (Shanghai, China).

2.4 Statistical analysis

The results were shown as mean ± standard deviation (SD). The values were analyzed by one-way analysis of variance (ANOVA) and Duncan's multiple range test. $P < 0.05$ was regarded as significant.

3. Results

3.1 ES preparation and its purification

As displayed in Fig. 2A, 4 fractions, named as ES1, ES2, ES3 and ES4, were collected by a DEAE Seplife FF chromatographic column. ES1, ES2, ES3 and ES4 account for 52.31%, 26.42%, 17.99% and 3.28%, respectively. In our work, the dominant fraction (ES1) was further purified by a Sephacryl S-400HR column (Fig. 2B). The elution curve showed a single and symmetrical peak, indicating that ES1 was the single and uniform fraction. After purification, the purity of ES1 reached 96.7%, while the protein content was not detectable.

3.2 Structural characterization of ES1

3.2.1 UV-Vis analysis of ES1

As shown in Fig. 2C, the UV-Vis spectrum revealed that ES1 had no absorption peaks at 260 and 280 nm, proving that there were no nucleic acid and protein in ES1.

3.2.2 FT-IR spectroscopy of ES1

As pictured in Fig. 2D, a strong absorption peak at 3 413.52 cm^{-1} and a faint absorption peak at 2 927.34 cm^{-1} were correspondence to the stretching vibrations of OH and C–H, respectively. Due to the stretching vibration of C=O, a weak absorption peak appeared at 1 643.51 cm^{-1}. The stretching vibration of C–H and C–O–C was represented by absorption peaks at 1 384.13 and 1 074.33 cm^{-1}, respectively. Furthermore, the absorption peak at 885.75 cm^{-1} testified that the structure of ES1 contained α-type glycosidic bonds.

3.2.3 Mw of ES1

Absolute *M*w analysis diagram was shown in Fig. 2E. After GPC-RI-MALS analysis, software ASTRA 6.1 was applied to calculate *M*w of ES1. The *M*w and number-average molecular weight (*M*n) of ES1 was 25.79 and 21.92 kDa. Its polydispersity index (*M*w/*M*n) was 1.177 indicating its homogeneity. Only a single peak was found in light scattering (LS) and refractive index (RI) detectors, suggesting no obvious aggregation of ES1. Furthermore, molecular configuration analysis diagram of ES1 produced a line with a slope of 1.09 ± 0.04 (Fig. S1), demonstrating that ES1 was a rodlike molecule.

3.2.4 Monosaccharide composition of ES1

Chromatogram charts of the standard and ES1 were displayed in Fig. 2F. Compared with the retention time of standard, ES1 was made up of Fuc, Gal, Glc and Man with the molar ratios of 1.00:2.25:1.01:1.01.

3.2.5 Glycosyl linkage types of ES1

Total ion profile and secondary mass spectrum of ES1 were shown in Figs. S2 and S3, respectively. On the basis of the retention times and standard data of partially methylated alditol acetates in the Complex Carbohydrate Research Center spectral database, the glycosidic linkage patterns of ES1 were identified and shown in Table 1. ES1 was mainly composed of 5 glycosidic residues (labelling: A–E) including Man*p*-(1→, Glc*p*-(1→, →3)-Fuc*p*-(1→, →6)-Gal*p*-(1→ and →2,6)-Gal*p*-(1→.

3.2.6 NMR analysis of ES1

1D NMR and 2D NMR spectra of ES1 were pictured in Fig. 3. The ^{1}H NMR spectrum was crowded in a range of δ3.0−δ5.5 (Fig. 3A). The chemical shift signals at δ3.2−δ4.0 were glycocyclic proton signals, while main anomeric proton signals (δ5.06, δ4.94, δ5.07, δ4.97 and δ4.99) were concentrated in a region of δ4.3−δ5.5 and named as A, B, C, D and E. The signal at δ1.17 indicated the existence of methyl-proton of Fuc. The ^{13}C NMR spectrum showed that the anomeric carbon signals at δ102.28, δ102.06, δ100.46 and δ98.7 were mainly

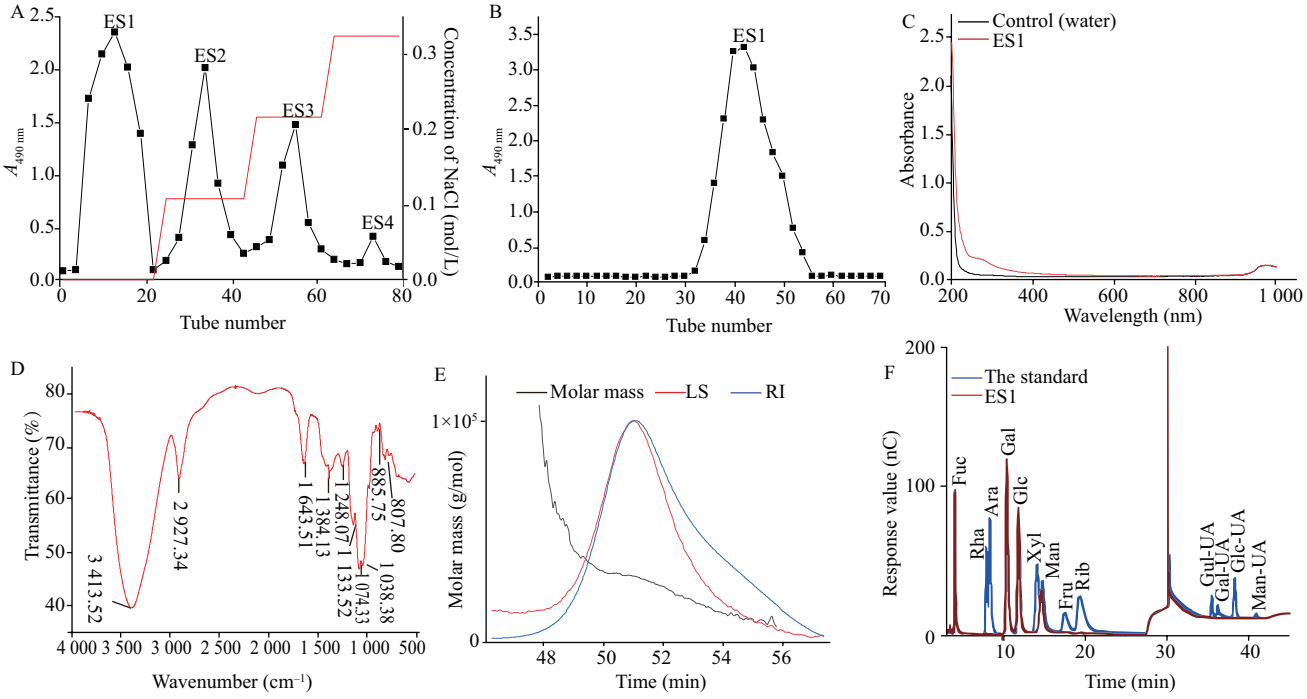

Fig. 2 Separation, purification and preliminary characterization of ES1. (A) Elution curve by a DEAE Seplife FF chromatographic column; (B) Elution curve by a Sephacryl S-400HR column; (C) UV-Vis; (D) FT-IR; (E) Absolute *M*w analysis diagram; (F) Chromatogram chart of the standard and ES1.

Table 1
Results of the methylation analysis of ES1.

Code	Retention time (min)	Methylation residues	Linkage patterns	Molar ratio	Major mass fragments (*m/z*)
A	8.994	2,3,4,6-Me_4-Man*p*	Man*p*-(1→	1.02	59, 71, 87, 102.1, 129, 145.1, 162.1, 174.1, 205.1
B	9.070	2,3,4,6-Me_4-Glc*p*	Glc*p*-(1→	1.00	60, 71, 87, 102, 118, 145.1, 162.1, 205.1
C	9.726	2,4-Me_2-Fuc*p*	→3)-Fuc*p*-(1→	1.00	59, 72, 89, 101, 118, 131.1, 141, 160.1, 187.1, 201.1
D	15.691	2,3,4-Me_3-Gal*p*	→6)-Gal*p*-(1→	1.19	71, 87, 102, 118, 129, 142, 162.1, 173.1, 189.1, 233.1
E	19.886	3,4-Me_2-Gal*p*	→2,6)-Gal*p*-(1→	1.42	59, 74, 87, 100, 114, 130, 143.1, 160.1, 190.1, 234.1

located between δ90 and δ110 (Fig. 3B). The main signal peaks of the sugar-ring were distributed in the region of δ60−δ85, and the signal at δ15.28 indicated the existence of methyl-carbon of Fuc.

For residue A in ^{1}H-^{1}H COSY spectrum (Fig. 3E), the chemical shift signals of H1/2, H2/3, H3/4, H4/H5, H5/6b and H6a/H6b from the cross peaks were at δ5.06/4.01, δ4.01/3.84, δ3.84/3.73, δ3.73/3.83, δ3.83/3.84 and δ3.84/3.70, respectively. Furthermore, residue A in HSQC spectrum had a cross-coupling resonance signal at δ5.06/102.06 (Fig. 3C), which was assigned to H1/C1 in the anomeric region of residue A. The chemical shift signals of H2/C2, H3/C3, H4/C4, H5/C5 and H6a/C6 were corresponded to δ4.01/69.78, δ3.84/67.2, δ3.73/73.22, δ3.83/69.4 and δ3.84/61. According to similar principle and combination with ^{1}H-^{13}C HMBC and ^{1}H-^{1}H COSY spectra, the chemical shift signals of all residue signals were attributed, and the data were shown in Table 2. Based on monosaccharide composition, methylation results, chemical shift signals and relevant literature[27-32], it can be inferred that the residues A, B, C, D and E were *α*-*D*-Man*p*-(1→, →2,6)-*α*-*D*-Gal*p*-(1→, →6)-*α*-*D*-Gal*p*-(1→, →3)-*α*-*L*-Fuc*p*-(1→ and *α*-*D*-Glc*p*-(1→, respectively.

Then, the sequence of glycoside linkage was analyzed by ^{1}H-^{13}C HMBC (Fig. 3D) and ^{1}H-^{1}H NOESY (Fig. 3F). For main chain analysis, H1 of residue C showed a signal peak (CH1/BC2) with C2 of residue B, indicating the presence of →6)-C-(1→2,6)-B-(1→. A correlated signal peak (BH1/DH3) between H1 of residue B and H3 of residue D showed the existence of →2,6)-B-(1→3)-D-(1→. A cross peak (DH1/BH2) between H1 of residue D and H2 of residue B proved the presence of →3)-D-(1→2,6)-B-(1→. H1 of residue B and H6 of residue C revealed a correlated signal peak (BH1/CH6a), displaying the existence of branched chain analysis, H1 of residue A had correlation signal peaks (AH1/BC6 and AH1/BH6a) with C6 and H6 of residue B, respectively, indicating the presence of A-(1→6,2)-B-(1→. A cross peak (EH1/BH6a) between H1 of residue E and H6a of residue B proved the existence of E-(1→6,2)-B-(1→. In summary, combined with monosaccharide components, methylation analysis and NMR data, the structural formula of ES1 was inferred in Fig. 3G.

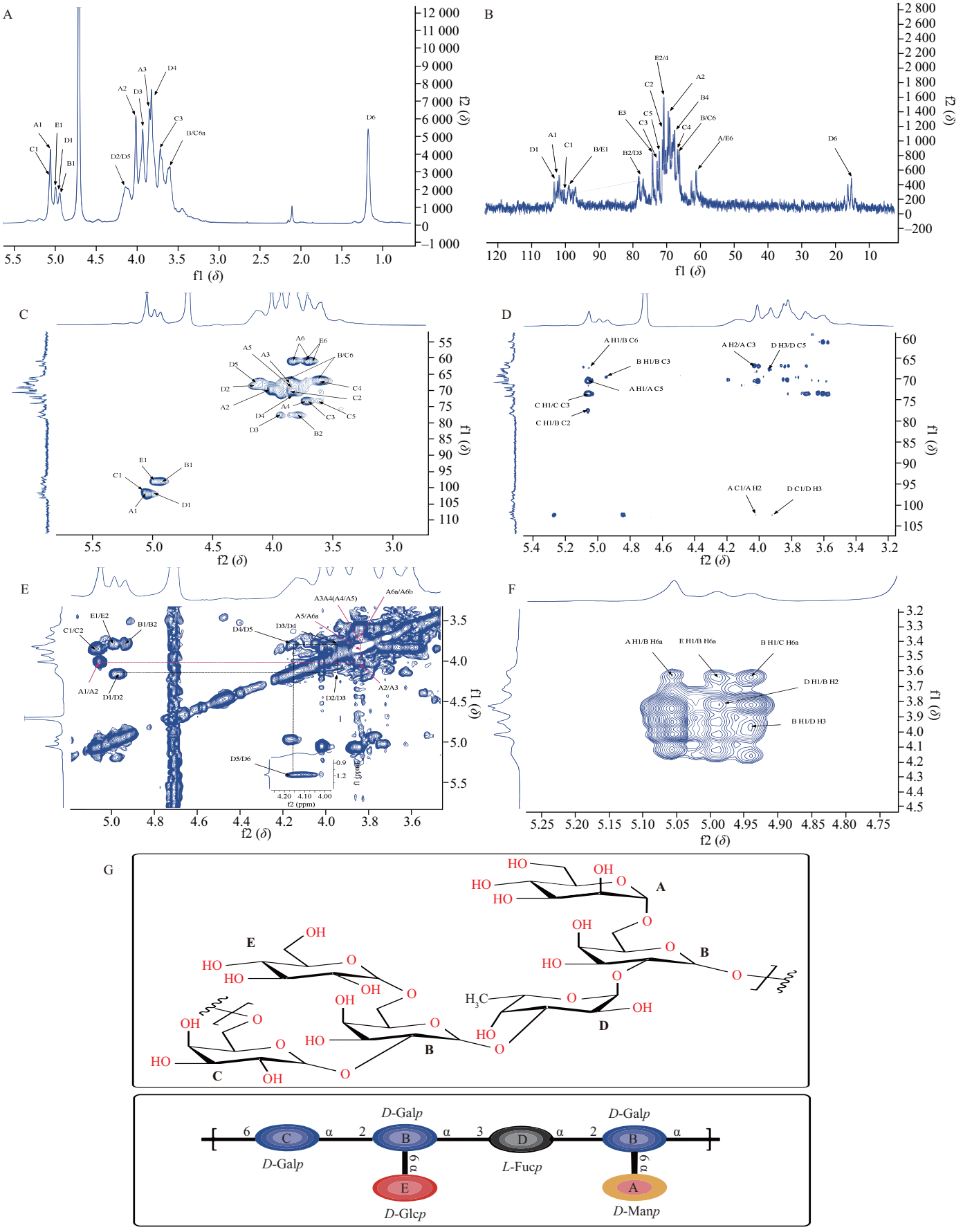

Fig. 3 NMR analysis of ES1. (A) ^{1}H NMR; (B) ^{13}C NMR; (C) ^{1}H-^{13}C HSQC; (D) ^{1}H-^{13}C HMBC; (E) ^{1}H-^{1}H COSY; (F) ^{1}H-^{1}H NOESY; (G) Predicted structure.

3.3 Hepatoprotective experiments of ES1 against chronic ALD in mice

3.3.1 ES1 alleviated chronic alcohol-induced liver injury

As shown in Fig. 4A, compared to NS group, chronic alcohol significantly increased liver index ($P < 0.05$), indicating that chronic alcohol had led to liver swelling. Interestingly, the supplement of ES1 obviously reversed this abnormal change ($P < 0.05$).

To assess degree of liver injury, serum AST and ALT were detected (Figs. 4B and C). The activities of AST and ALT in EtOH group were observably boosted ($P < 0.05$), compared with NS group, proving that chronic alcohol had caused hepatic injury and the ALD model was established successfully. Whereas ALT and AST activities in ES group were decreased remarkably ($P < 0.05$), explaining that ES1 could improve liver damage. To further evaluate the effect of ES1 on liver injury in ALD mice, hepatic histopathology by H&E staining was performed (Fig. 4G). The hepatocytes of mice in NS group showed a normal structure, such as orderly arrangement around the central vein, regular round nuclei, clear intercellular spaces, distinct cell boundaries and no lesions. However, liver sections of mice in EtOH group exhibited severe lesions, such as blurred cell boundaries, necrocytosis, karyopyknosis, membranolysis, dispersed vesicular steatosis and massive fat vacuoles. After the administration of ES1, steatosis, fat vacuoles and other lesions had been alleviated to a certain extent, further confirming that ES1 had the ability to reduce liver damage in ALD mice.

3.3.2 ES1 ameliorated blood lipid levels in ALD mice

As displayed in Figs. 4D-F, in comparison with NS group, serum TC and TG levels in EtOH group were significantly increased ($P < 0.05$), and serum HDL-C level was obviously decreased ($P < 0.05$), showing that dyslipidemia had occurred in ALD mice. However, ES1 administration visibly reduced TC and TG levels ($P < 0.05$), and observably upregulated HDL-C level ($P < 0.05$). These results indicated that ES1 could effectively maintain the normal transport pathway of cholesterol against metabolism disorder.

Table 2
Chemical shifts of ES1 in ^{1}H and ^{13}C NMR spectra.

Code	Glycosyl residues	Chemical shifts (δ)						
		H1/C1	H2/C2	H3/C3	H4/C4	H5/C5	H6a/C6	H6b
A	*α-D*-Man*p*-(1→	5.06	4.01	3.84	3.73	3.83	3.84	3.70
		102.06	69.78	67.20	73.22	69.40	61.00	–
B	→2,6)-*α-D*-Gal*p*-(1→	4.94	3.79	3.81	3.83	3.74	3.61	3.84
		98.07	77.62	69.78	67.20	73.22	66.40	–
C	→6)-*α-D*-Gal*p*-(1→	5.07	3.86	3.71	3.61	3.63	3.60	3.84
		100.46	70.37	73.22	66.77	72.79	66.5	–
D	→3)-*α-L*-Fuc*p*-(1→	4.97	4.16	3.94	3.82	4.15	1.17	–
		102.28	68.62	77.60	72.10	67.90	15.28	–
E	*α-D*-Glc*p*-(1→	4.99	3.80	3.72	3.42	3.40	3.65	3.74
		98.07	70.08	74.10	70.80	67.50	61.00	–

Note: The symbol "–" indicates the absence of a chemical shift.

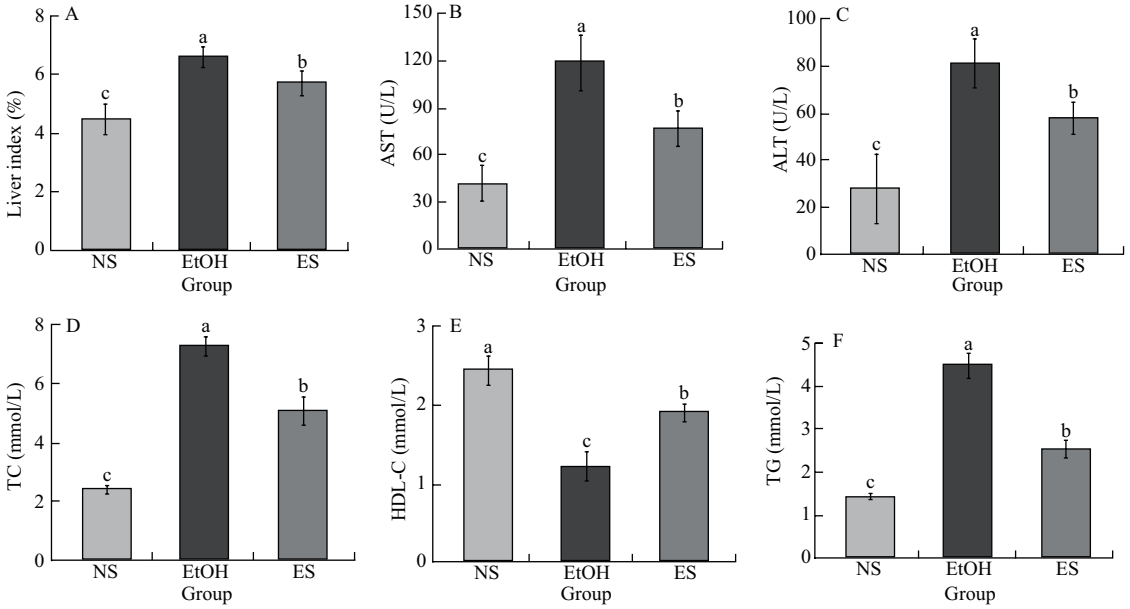

Fig. 4 Effect of ES1 on hepatic injury in ALD mice. (A) Liver index; (B) AST; (C) ALT; (D) TC; (E) HDL-C; (F) TG; (G) Histological analysis (H&E, 100×, 200× and 400×; scale bar = 100, 50 and 20 μm). Yellow arrow represented diffuse vesicular steatosis and red arrow represented vacuolar degeneration. The values are reported as means ± SD. Bars with different letters are significantly different ($P < 0.05$).

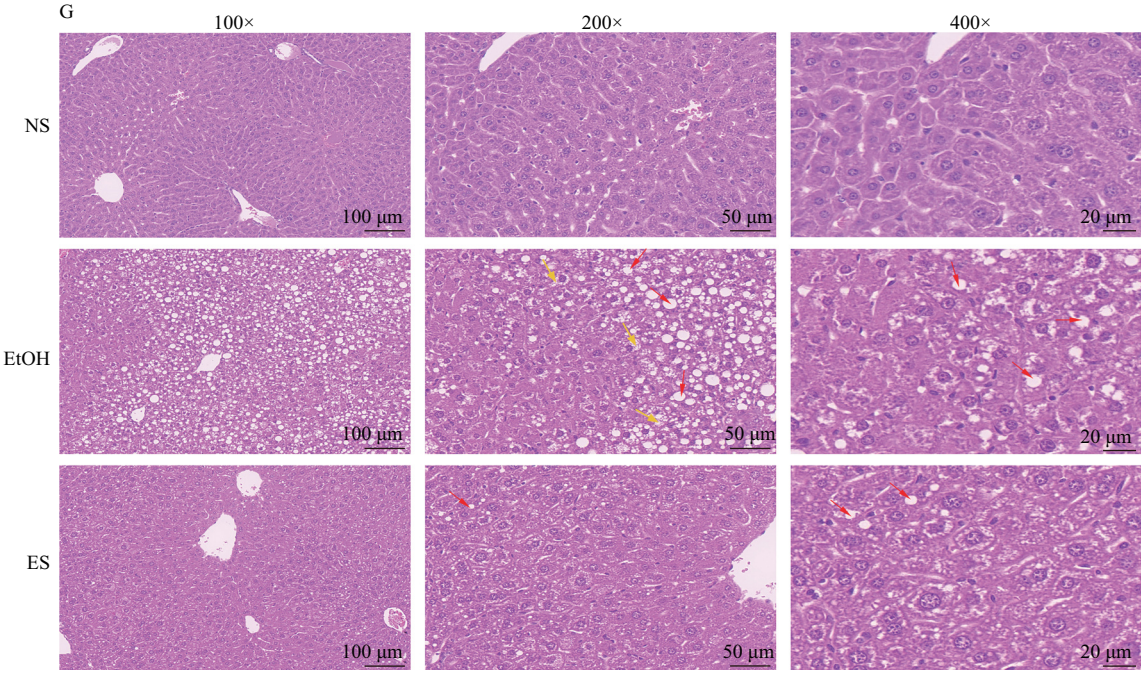

Fig. 4 (*Continued*)

3.3.3 ES1 regulated P62/Nrf2 pathway to inhibit hepatic oxidative stress in ALD mice

To assess effect of ES1 on chronic alcohol-induced oxidative stress, SOD, GSH-Px, CAT and MDA were tested (Figs. 5A-D). Compared to NS group, chronic alcohol apparently decreased SOD, GSH-Px and CAT activities ($P < 0.05$), and markedly increased MDA level ($P < 0.05$), illustrating that antioxidant system in liver had been destroyed to cause oxidative stress. Compared to EtOH group, the supplement of ES1 distinctly enhanced antioxidant enzymes activities ($P < 0.05$), and obviously reduced MDA level ($P < 0.05$). The above results showed that ES1 could increase antioxidant enzymes to suppress chronic alcohol-induced oxidative stress.

To observe intuitively effect of ES1 on chronic alcohol-induced oxidative stress, ROS was marked by dihydroethidium, and labeled ROS was red (Figs. 5E and F). The results showed that ROS levels in EtOH group were higher than those in NS group ($P < 0.05$), indicating that chronic alcohol administration could contribute to ROS accumulation in liver. However, in comparison with those of EtOH group, ROS levels in ES group were obviously decreased ($P < 0.05$), showing that ES1 treatment could inhibit ROS generation in ALD mice. In conclusion, from both perspectives of antioxidase and ROS, ES1 could mitigate chronic alcohol-induced hepatic oxidative stress.

To further explore the mechanism of ES1 against hepatic oxidative stress, we evaluated the classical signaling pathway (P62/Nrf2) in antioxidant system (Figs. 5G-L). Compared to NS group, SOD1, NQO1 and glutathione peroxidase 1 (GPx-1) expressions in EtOH group were significantly down-regulated ($P < 0.05$), whereas Nrf2 expression was visibly up-regulated ($P < 0.05$). These results suggested that although the antioxidant system could be temporarily activated, antioxidase expressions have been reduced. However, ES1 obviously activated Nrf2 signaling pathway to increase SOD1, NQO1 and GPx-1 expressions ($P < 0.05$), in comparison with those in EtOH group, which was in accordance with the immunofluorescence result of Nrf2 (Fig. S4). Interestingly, ES1 also upregulated the expression of P62 ($P < 0.05$). To sum up, ES1 could activate Nrf2 signaling pathway and P62 (a positive feedback circuit) to enhance antioxidase activities for defending chronic alcohol-induced hepatic oxidative stress.

3.3.4 ES1 regulated AMPK pathway to improve abnormal hepatic lipid in ALD mice

As shown in Fig. 6A, no obvious lipid droplets were found in liver of mice from NS group, whereas dense red fat droplets appeared in liver of mice from EtOH group, indicating that the liver in ALD mice had developed severe lipid metabolism disorders. However, the accumulation of red lipid droplets in liver of mice in ES group was improved, and the density was also reduced. These results testified that ES1 could effectively ameliorate lipid metabolism disorder in ALD mice.

To further verify effect of ES1 on hepatic lipid metabolism disorder in ALD mice, hepatic TC and TG were detected. As displayed in Figs. 6B and C, compared with NS group, TC and TG levels in EtOH group were clearly elevated ($P < 0.05$), testifying that hepatic lipid metabolism disorder had occurred in ALD mice. Moreover, the treatment with ES1 obviously decreased TC and TG levels ($P < 0.05$). These results further indicated that ES1 could improve hepatic lipid metabolism disorder by inhibiting fat accumulation in liver of ALD mice.

To further explore the mechanism of ES1 against chronic alcohol-induced the disorder of lipid metabolism, we assessed the AMPK pathway including AMPK, p-AMPK PPARα, SREBP-1, fatty acid synthase (FAS) and stearoyl-CoA desaturase (SCD). As pictured in Figs. 6D-I, in comparison with NS group, AMPK phosphorylation level and PPARα expression in EtOH group were significantly suppressed ($P < 0.05$), and the expressions of SREBP-1, FAS and SCD were distinctly increased ($P < 0.05$), proving that AMPK pathway was inhibited by chronic alcohol. However, these abnormal changes were signally improved by ES1 administration ($P < 0.05$). These results showed that ES1 could regulate AMPK pathway to reduce fat accumulation against lipid metabolism disorder.

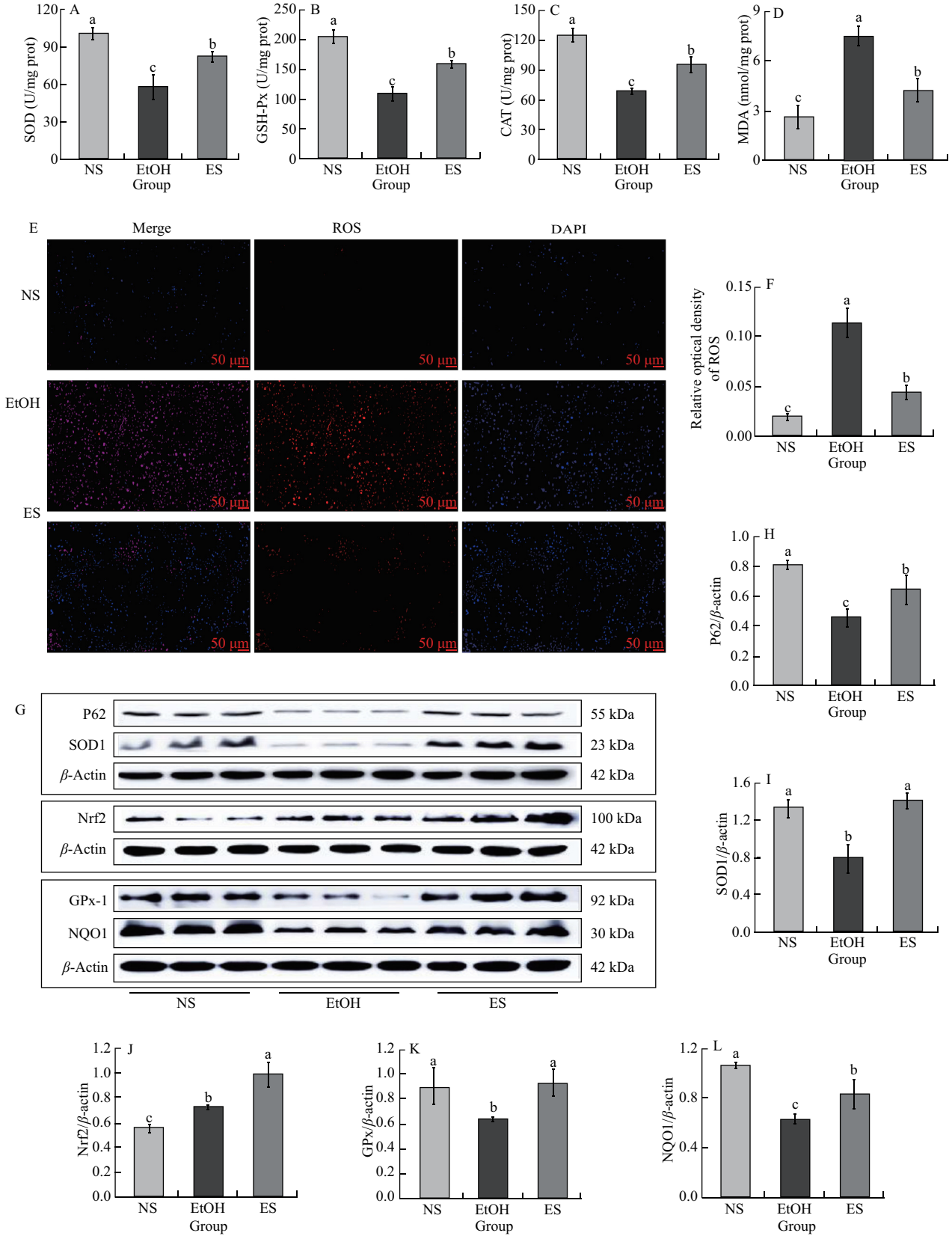

Fig. 5 ES1 enhanced hepatic antioxidant capacity by P62/Nrf2 pathway in ALD mice. (A) SOD; (B) GSH-Px; (C) CAT; (D) MDA; (E) ROS in mouse liver tissues from each group (200×, scale bar = 50 μm); (F) Semi-quantitative analysis of ROS; (G) P62, SOD1, Nrf2, GPx-1 and NQO1 levels were evaluated by Western blot in liver; (H-M) Semi-quantitative analysis of P62, SOD1, Nrf2, GPx-1 and NQO1 by ImageJ. The values are reported as means ± SD. Bars with different letters are significantly different ($P < 0.05$).

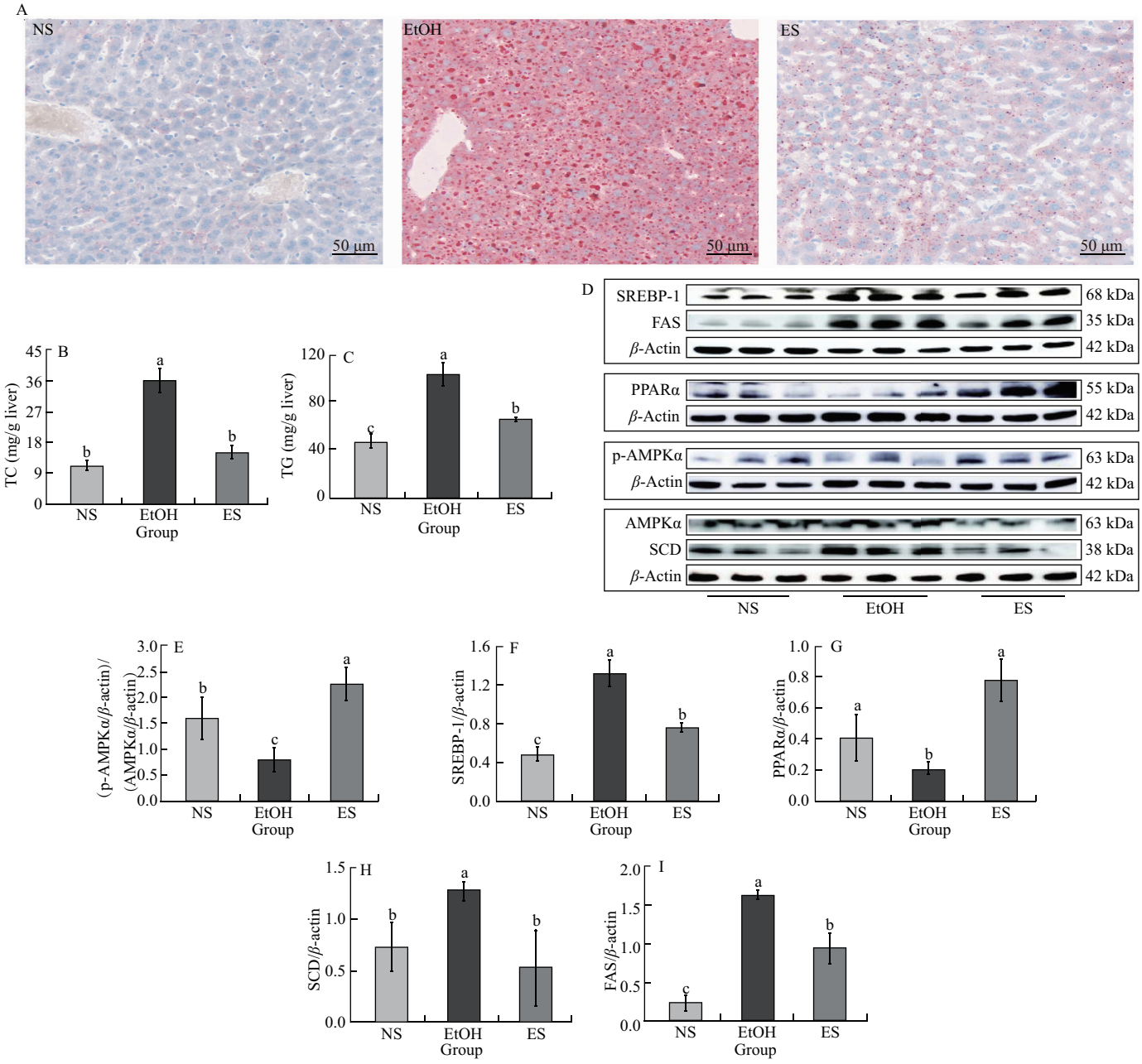

Fig. 6 ES1 inhibited abnormal hepatic lipid by AMPK pathway in ALD mice. (A) Oil red O staining (200×, scale bar = 100 μm); (B) TC; (C) TG; (D) AMPK, p-AMPKα, SREBP-1, PPARα, SCD and FAS levels were evaluated by Western blot in liver; (H-M) Semi-quantitative analysis of p-AMPKα/AMPKα, SREBP-1, PPARα, SCD and FAS by ImageJ. The values are reported as means ± SD. Bars with different letters are significantly different ($P < 0.05$).

3.3.5 ES1 improved the structure of the gut microbiota in ALD mice

After 16S rRNA sequencing of mouse fecal microorganisms were optimized and analyzed, sequence number was 665 447, base number was 281 915 664 bp, and average length was 423 bp. The sequences were classified into different operational taxonomic units (OTUs) (similarity > 97%), and we conducted correlation analysis on the number of unique and common OTU in the intestinal flora of mice in each group. As demonstrated in Fig. S5A, the OTU number in NS, EtOH and ES groups were 273, 395 and 487, respectively. and the mutual number of OTU in each group was 122, showing that the similarity of intestinal flora in each group was different.

With the gradual increase in the number of samples, Pan and Core curves showed flattening (Figs. S5B and C), testifying that sample number was competent for this analysis. Furthermore, Rank-Abundance curve showed that ES group had the highest species richness among 3 groups, and the species distributions of 3 groups were relatively uniform (Fig. S5D). Meantime, with number of reads sampled increased, rarefaction curves of Sobs and Shannon in 3 groups became slower gradually (Figs. 7A and B), indicating that the measured data in this experiment was reasonable, and the amount of sequencing data was sufficient to reflect the vast majority of microbial diversity in all samples. In conclusion, the amount of sequencing data was true reliability and the sequencing depth was enough.

Partial least squares discriminant analysis (PLS-DA) showed that OUT levels between NS group and EtOH group and between EtOH group and ES group could be well separated (Fig. 7C), indicating that alcohol or ES1 was indeed a major factor affecting the grouping. ANOSIM/Adonis displayed that difference between groups were obviously higher than those within the group (Fig. 7D), further demonstrating PLS-DA result.

As exhibited in Figs. 7E-H, Sobs, Chao, Ace and Shannon indexes in EtOH group were distinctly increased ($P < 0.05$), in comparison with those in NS group, while Simpson index was markedly decreased. Interestingly, there were significant differences in the indexes of Sobs, Chao and Ace between EtOH group and ES group. Meantime, Coverage index in three groups were all > 0.998, showing that sequencing results represented the real situation of microorganisms in all samples. These results showed that alcohol or ES1 could affect the richness and diversity of gut flora in ALD mice to a certain extent.

Principal component analysis (PCA), principal coordinates analysis (PCoA) and non-metric multidimensional scaling (NMDS) were demonstrated in Figs. 7I-K. Gut microbiota composition between NS group and EtOH group showed a clear trend of separation, indicating that alcohol treatment had altered the composition of gut microbes. However, the supplement of ES1 caused a significant difference in the composition of gut microbes between EtOH group and ES group, proving that ES1 could improve intestinal microbial disturbances in ALD mice. Meantime, hierarchical clustering analysis also confirmed the results of PCA, PCoA and NMDS (Fig. 7L).

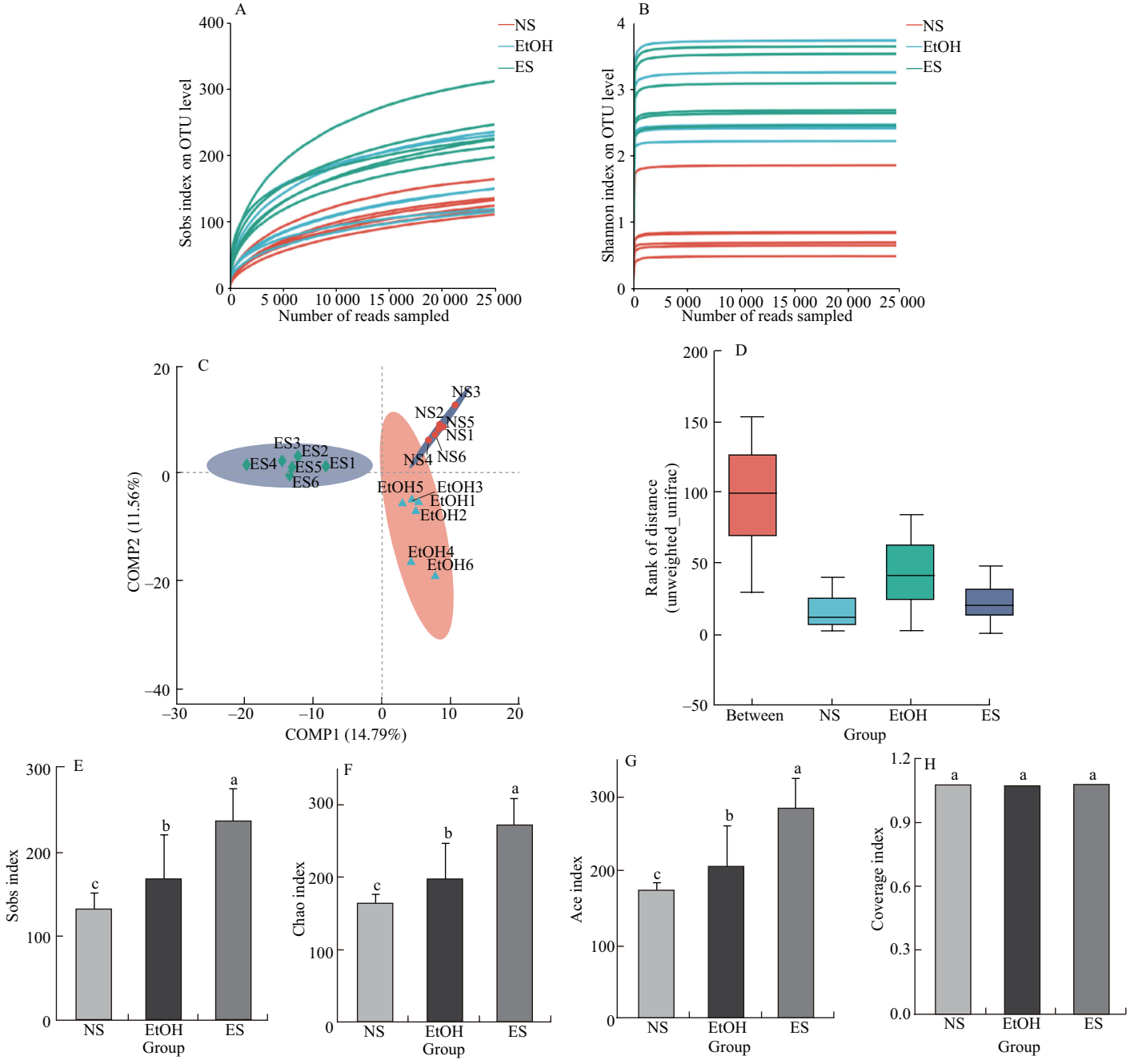

Fig. 7 Dilution curve, between-group similarity analysis, α-diversity analysis and β-diversity analysis. (A) Rarefaction curve of Sobs; (B) Rarefaction curve of Shannon; (C) PLS-DA analysis at the OTU levels; (D) ANOSIM/Adonis analysis based on Unweighted_unifrac at the OTU levels; (E) Sobs; (F) Chao; (G) Ace; (H) Coverage; (I) PCA; (J) PCoA; (K) NMDS; (L) Hierarchical clustering tree. The values are reported as means ± SD. Bars with different letters are significantly different ($P < 0.05$).

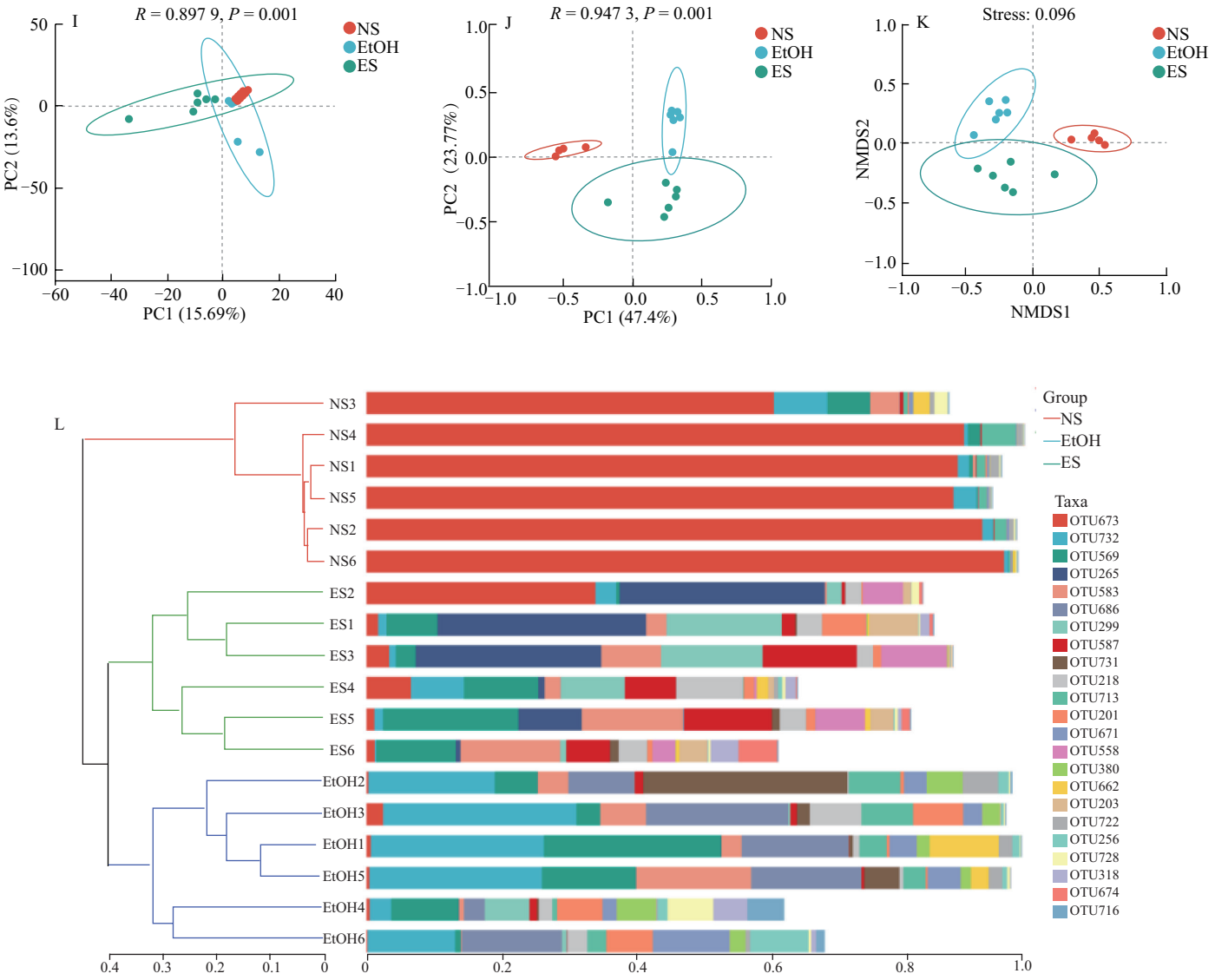

Fig. 7 (*Continued*)

Percent of community abundance, Circos diagram and relative abundance table at phylum level showed that Firmicutes, Bacteroidota, Actinobacteriota, Proteobacteria, Verrucomicrobiota, Deferribacterota, Campylobacterota, Desulfobacterota, Patescibacteria and Cyanobacteria were dominant phyla among three groups (Figs. 8A, S5E and Table S2). The heatmap clustering analysis was more intuitive to observe significant differences among 3 groups at phylum level (Fig. 8B). To further analyze changes at phylum level, we assessed the differences between the 2 groups (Figs. 8C and D). Compared to NS group, the relative abundances of Actinobacteriota and Proteobacteria in EtOH group were obviously increased ($P < 0.05$). Interestingly, in comparison with EtOH group, the relative abundance of Verrucomicrobiota was distinctly raised in ES group ($P < 0.05$). These results indicated that gut microbiota at phylum level was clearly regulated by ES1 in ALD mice.

Proportion of community abundance, Circos diagram and relative abundance table at genus level displayed that *Ligilactobacillus*, *Monoglobus*, *Dubosiella*, *Staphylococcus*, *Allobaculum*, *Jeotgalicoccus*, norank_f_Muribaculaceae, *Psychrobacter*, *Aerococcus* and *Limosilactobacillus* were dominant genera among 3 groups (Figs. 8E, S5F and Table S3). Heatmap clustering analysis showed visible differences among 3 groups at genus level (Fig. 8F). Compared with NS group, the relative abundance of *Ligilactobacillus* was significantly reduced, while the relative abundances of *Dubosiella*, *Staphylococcus*, *Allobaculum*, *Psychrobacter*, *Jeotgalicoccus*, *Faecalibaculum*, Coriobacteriaceae_UCG-002, *Romboutsia* and *Enterococcus* were significantly elevated ($P < 0.05$) in EtOH group (Fig. 8G). However, ES1 administration increased obviously the relative abundances of *Monoglobus*, *Ligilactobacillus*, *Aerococcus* and *Akkermansia* ($P < 0.05$), and decreased remarkably the relative abundances of Coriobacteriaceae_UCG-002, *Faecalibaculum*, *Limosilactobacillus*, *Dubosiella* and *Romboutsia* UCG-002 (Fig. 8H, $P < 0.05$). Meantime, linear discriminant analysis effect size (LEfSe) analysis was used to further test differences of species

abundance between groups (Figs. 8I-J, and S5G, H). Compared to NS group, *Staphylococcus*, *Psychrobacter*, *Dubosiella*, *Allobaculum*, *Jeotgalicoccus*, *Faecalibaculum*, *Enterococcus* and *Romboutsia* in EtOH group were core genera. Compared with EtOH group, *Monoglobu*, *Ligilactobacillus*, *Akkermansia*, NK4A214_group, *Aerococcus* and unclassified_f_Lachnospiraceae were core genera. These results indicated that ES1 could alleviate intestinal microecology imbalance at genus level to some extent in ALD mice.

3.3.6 *Association analysis of clinical factors*

Distance-based redundancy analysis (db-RDA) was shown in Fig. 8K. Acute angles among serum AST ALT and hepatic TC, TG, ROS and MDA indicated that they were positive correlations, and hepatic CAT, GSH-Px and SOD were positive correlations. CAT, GSH-Px and SOD were with AST, ALT, TC, TG and ROS at an obtuse angle, showing that the first 3 were negatively correlated with the last 5. Meantime, we found that genera in EtOH group had more influence on changes of AST, ALT, TC, TG, ROS and MDA, while genera in ES group had more influence on changes of hepatic CAT, GSH-Px and SOD. These results were consistent with the previous conclusions of biochemical indicators in EtOH group, as well as opposite results in ES group, testifying that changes in gut microbiome caused by ES1 supplementation could improve relevant biochemical indexes in ALD mice.

A heatmap of Spearman's correlation analysis between relevant biochemical indexes (AST, ALT, TC, TG, ROS, CAT, GSH-Px and SOD) and gut microbiota at genus level was exhibited in Fig. 8L. *Ligilactobacillus* was positively correlated with CAT, GSH-Px and SOD, and negatively correlated with AST, ALT, TC, TG and ROS. *Enterococcus*, *Romboutsia*, *Allobaculum*, Coriobacteriaceae_UCG-002, *Dubosiella* and *Faecalibaculum* were positively correlated with AST, ALT, TC, TG and ROS, and negatively correlated with CAT, GSH-Px and SOD. Hence, some key genera in gut microbiota played an important role in occurrence and development of ALD.

3.3.7 *ES1 restored the intestinal barrier in ALD mice*

As illustrated in Fig. 9A, the colonic tissues of mice in NS group showed a normal structure, such as normal crypt structure, orderly arrangement of goblet cells, intact colon epithelium and no other lesions. However, chronic alcohol had caused colonic tissue injury including obvious inflammatory infiltration, decreased and disorganized goblet cells, atrophic crypt. Interestingly, the supplement of ES1 markedly alleviated these abnormal changes, demonstrating that ES1 could mitigate colonic tissue injury in ALD mice.

To further explore whether ES1 could protect the intestinal barrier in ALD mice, zonula occludens-1 (ZO-1), Occludin and Claudin1 were examined. As displayed in Figs. 9B-E, compared to NS group, ZO-1, Occludin and Claudin1 expressions in EtOH group were obviously down-regulated ($P < 0.05$), proving that intestinal barrier was destructed. However, ES1 significantly up-regulated ZO-1, Occludin and Claudin1 expressions in comparison with EtOH group ($P < 0.05$). In a word, these results manifested that ES1 could alleviate chronic alcohol-induced colonic injury.

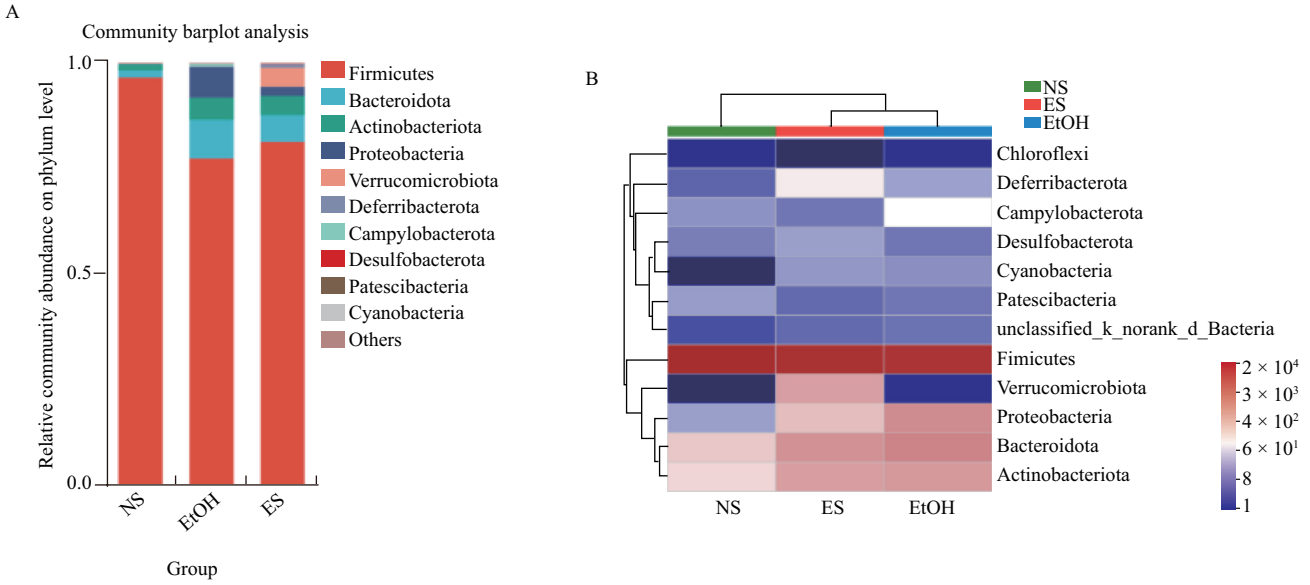

Fig. 8 Composition analysis in gut microbiota at the phylum and genus levels, and association analysis of clinical factors. (A) Community bar plot at phylum level; (B) Community heatmap analysis at phylum level; (C) Wilcoxon rank-sum test bar plot (NS *vs*. EtOH) based on Wilcoxon rank-sum test at phylum level; (D) Wilcoxon rank-sum test bar plot (EtOH *vs*. ES) based on Wilcoxon rank-sum test at phylum level; (E) Community bar plot at genus level; (F) Community heatmap analysis at genus level; (G) Wilcoxon rank-sum test bar plot (NS *vs*. EtOH) based on Wilcoxon rank-sum test at genus level; (H) Wilcoxon rank-sum test bar plot (EtOH *vs*. ES) based on Wilcoxon rank-sum test at genus level; (I) Histogram between NS group and EtOH group (LDA scores > 4); (J) Histogram between EtOH group and ES group (LDA scores > 4); (K) db-RDA analysis at genus level; (L) Heatmap of Spearman's correlations analysis between relevant biochemical indexes and gut microbiota at genus level. *$P < 0.05$, **$P < 0.01$, ***$P < 0.001$, indicating statistically significant differences between gut microbiota and clinical factors.

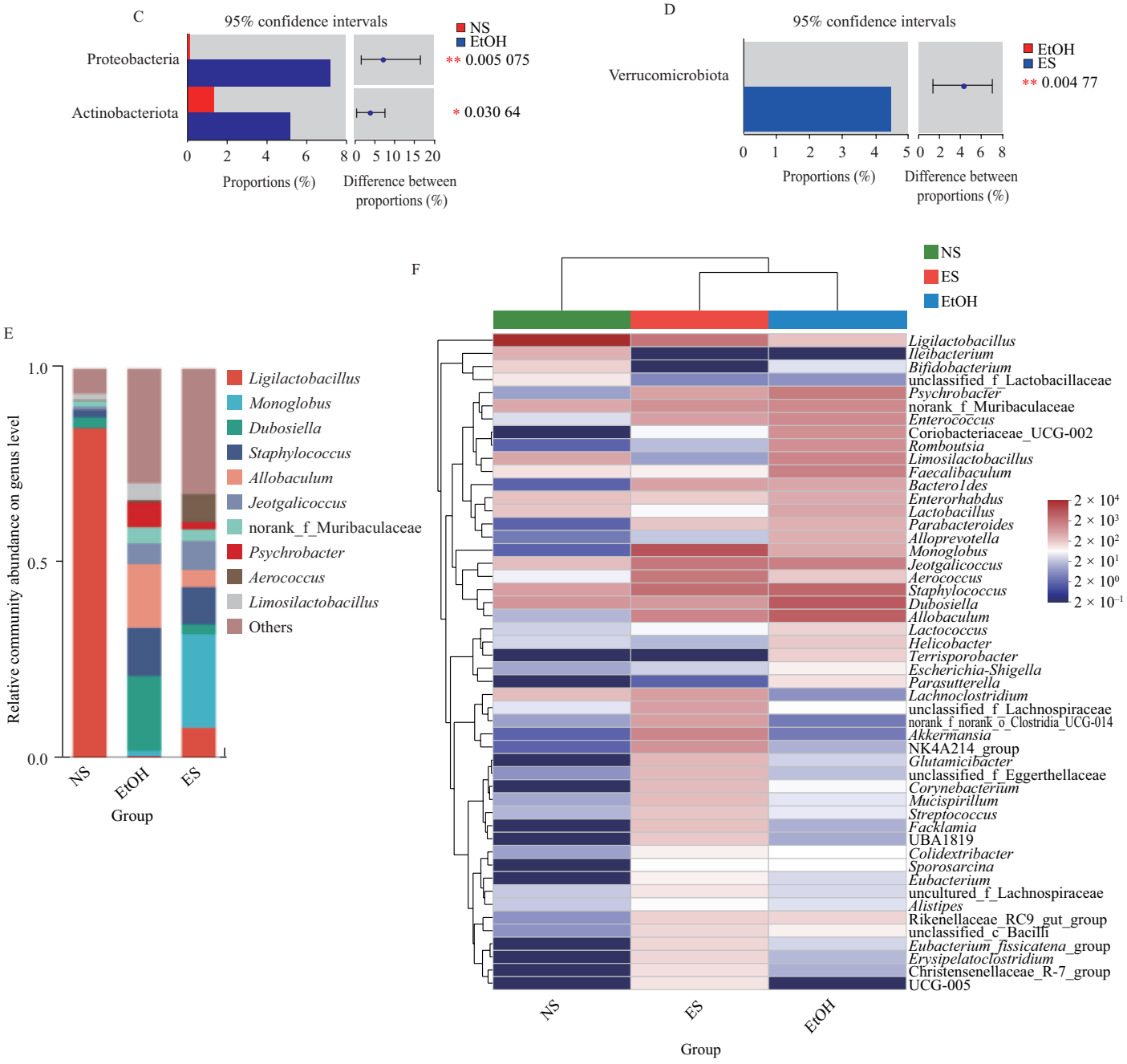

Fig. 8 (*Continued*)

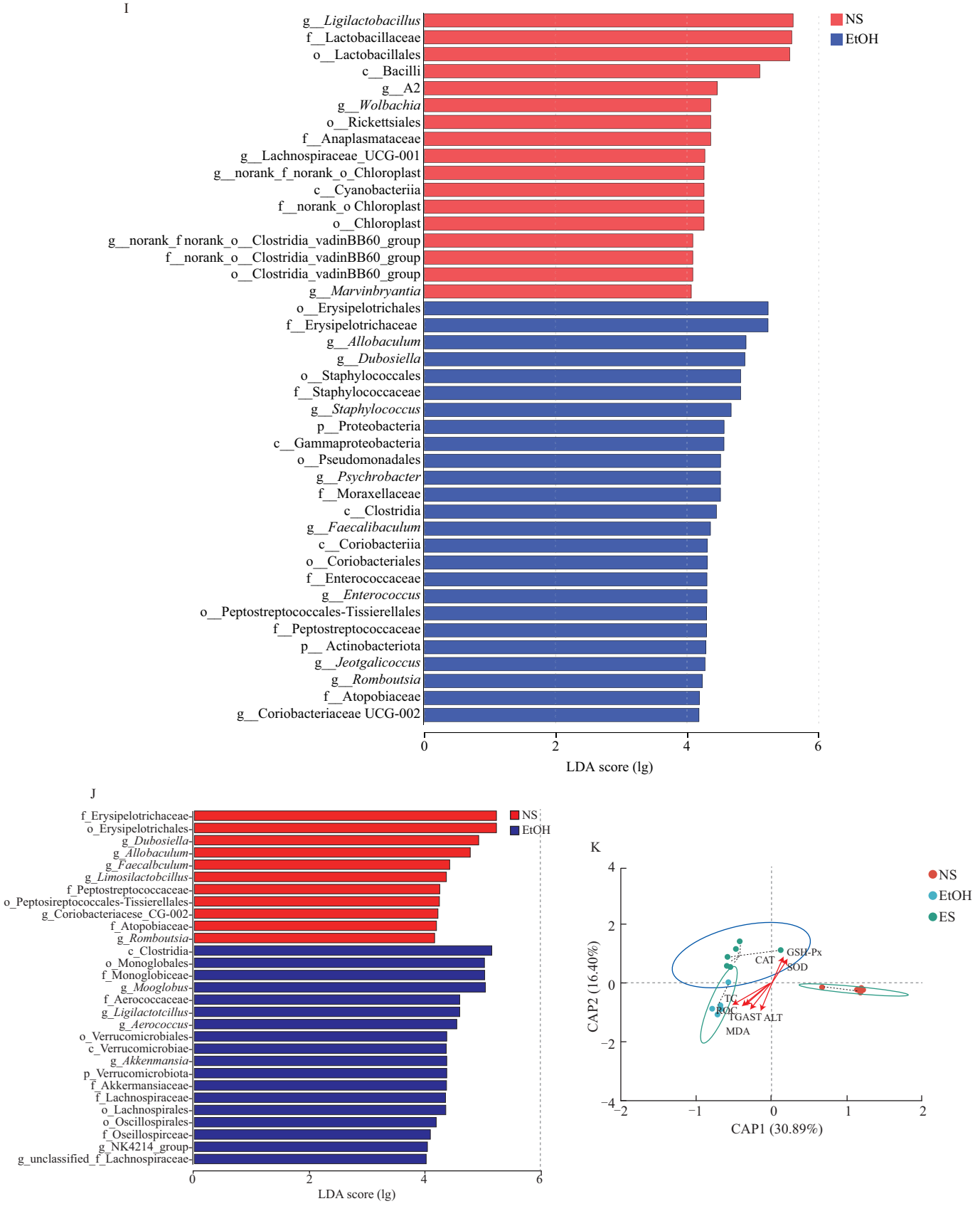

Fig. 8 (*Continued*)

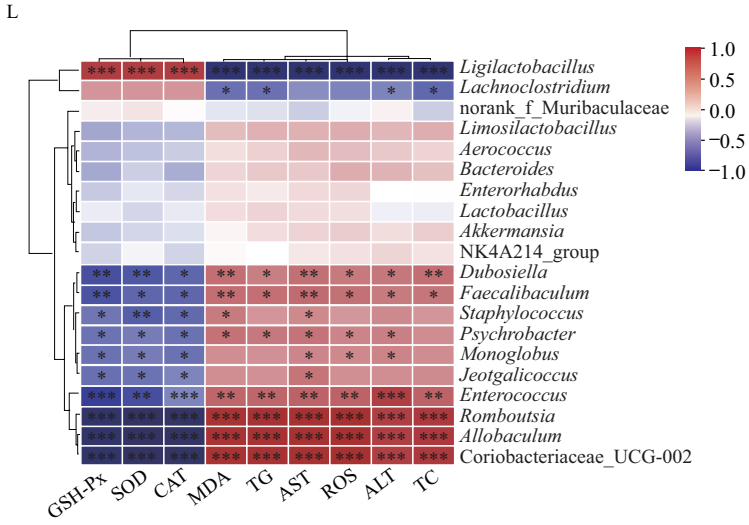

Fig. 8 (*Continued*)

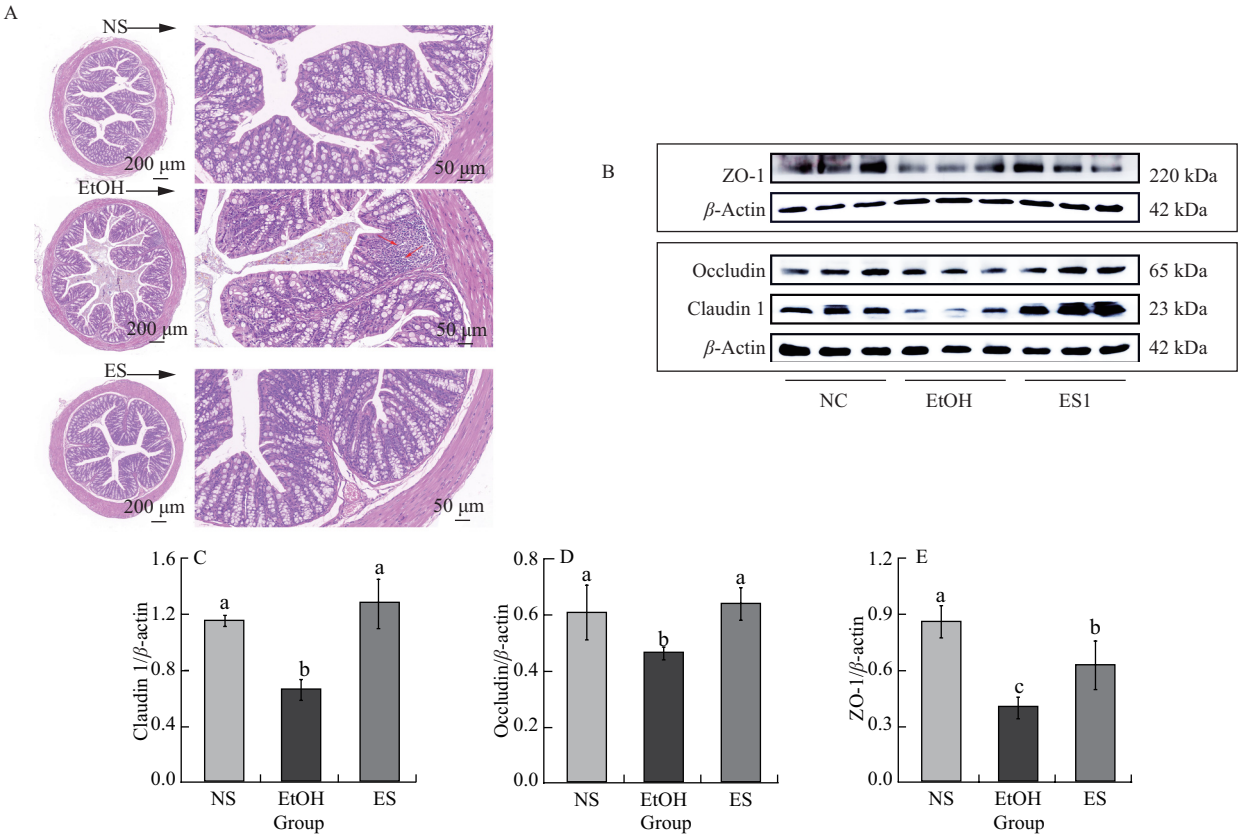

Fig. 9 ES1 restored the intestinal barrier in ALD mice. (A) Histological analysis for colon (H&E magnification 50× and 200×; scale bar = 200 and 50 μm). Red arrow represented inflammatory infiltration; (B) Claudin1, Occludin and ZO-1 levels were evaluated by Western blot in colon; (C-E) Semi-quantitative analysis of Claudin1, Occludin and ZO-1 by ImageJ. The values are reported as means ± SD. Bars with different letters are significantly different ($P < 0.05$).

4. Discussion

With the change of dietary structure and social intercourse expansion, alcohol consumption has increased rapidly, which caused that the incidence and mortality of ALD are increasing year by year[33]. Although the research on ALD pathogenesis has made breakthrough progress, there is no significant change in the effective treatment of ALD. However, natural substances for treating and preventing ALD have attracted the attention of researchers hoping to change the previous treatment approach, such as polysaccharides. In this work, ES was yielded by enzymatic-extractable method, and a new water-soluble polysaccharide (ES1) was obtained by DEAE Seplife FF and Sephacryl S-400HR columns. ES1 consisted of *α-D*-Man*p*-(1→, →2,6)-*α-D*-Gal*p*-(1→, →6)-*α-D*-Gal*p*-(1→, →3)-*α-L*-Fuc*p*-(1→, and *α-D*-Glc*p*-(1→, and its structure was inferred. Meantime, its effect against ALD as well as underlying mechanism was evaluated.

Modern medical research shows that the successful establishment of standardized animal models have laid a foundation for mechanism study of ALD. At present, the known animal models of alcoholic liver injury mainly involve the following ways: models of adding alcohol to drinking water, Tsukamato French animal models, Lieber-DeCarli animal models and models by alcohol gavage. For models of adding alcohol to drinking water, although the animal mortality is reduced, it is difficult to evaluate and control the role of nutritional factors in ALD. For models by alcohol gavage, the way of alcohol intake is inconsistent with human pathogenesis, and it is easy to pour alcohol into trachea for resulting in animal death. For Tsukamato French animal models, it is not in line with the normal alcohol intake path, and the operation is complicated and the price is expensive, thereby limiting the promotion and application. For Lieber-DeCarli animal models, this model allows animal to automatically drink alcoholic liquid feed, which has a high formation rate and good stability, and can replicate alcoholic fatty liver and hepatitis. Its advantage is that it can actively control the energy intake and maintain the energy balance between groups, thereby excluding the influence of energy imbalance on the experimental results. To better replicate ALD, Lieber-DeCarli ethanol liquid diet was used for establishing ALD model in our work.

The elevations of AST and ALT are important indexes to evaluate successful establishment of ALD model[34]. In our study, AST and ALT in EtOH group were obviously increased, indicating that the model was successfully established, which was consistent with the relevant reports[35]. Meantime, histopathological observations in EtOH group also showed that liver injury had occurred in ALD model. However, ES1 markedly decreased AST and ALT activities, and observably improved characteristics of liver injury, indicating that ES1 could mitigate chronic alcohol-induced liver injury. Some reports also have verified that polysaccharides play an important role in reducing AST, ALT activities and relieving characteristics of liver injury[1,3,26].

Long-term excessive intake of alcohol can disrupt the balance of the liver's antioxidant defense system for forming oxidative stress, thereby leading to liver damage[36]. Hence, inhibiting oxidative stress is effective measure against ALD. As the main product of hepatic lipid peroxidation, the overexpression of MDA can cause hepatocyte damage[37]. SOD, GSH-Px and CAT play a crucial role in improving lipid peroxidation and maintaining the structure and function of cell membrane by reducing ROS formation[38]. In our work, SOD, GSH-Px and CAT activities were observably decreased, and the levels of MDA and ROS were signally increased in ALD mice, which was consistent with previous report[39]. However, ES1 could enhance SOD, GSH-Px and CAT activities, and reduce MDA and ROS levels to inhibit alcohol-induced oxidative stress, which was in accordance with *Cistanche deserticola* polysaccharides and *Radix Puerariae lobatae* polysaccharides[26,40]. Furthermore, many evidences have showed that activation of Nrf2 pathway plays an important role in inhibiting oxidative stress caused by alcohol[1]. It has been reported that under oxidative stress, edible mushroom polysaccharides can trigger Nrf2 for balancing the damage of free radicals and stabilizing the redox dynamic balance[41]. In this study, the potential mechanism of ES1 activating antioxidant enzymes was further clarified, and the conclusion was consistent with the above. ES1 could indeed promote the nuclear translocation of Nrf2 to enhance some antioxidases (NQO1, SOD1, GPx-1) for exerting antioxidant capacity. Furthermore, activated Nrf2 may elevate SQSTM1/P62 expression, and upregulated SQSTM1/P62 reversely further activate Nrf2 for enhancing antioxidant capacity[10,42]. Interestingly, ES1 also increased P62 expression in ALD mice. Similar studies have reported that some natural substances can regulate P62-Nrf2 pathway to inhibit oxidative stress[6,43]. Meantime, Nrf2 was identified as the downstream signal of AMPK in oxidative stress, and it has been confirmed that AMPK activation can promote Nrf2 expression[44-45]. Some reports also have shown that ROS contribute to the ubiquitination and degradation of AMPK, which depended on the phosphorylation of AMPK in human and mouse models, and alcohol metabolism-generated ROS can decrease the level of AMPK phosphorylation[46]. In our work, we indeed observed that alcohol exposure inhibited AMPK phosphorylation, showing that a metabolic dysfunction and direct impairment of protein synthesis were affected by alcohol. However, ES1 markedly increased the level of AMPK phosphorylation against alcohol-induced oxidative stress. These results indicated that AMPK/Nrf2 pathway played an important role in which ES1 regulated antioxidases against liver damage in ALD mice. Similar studies also have reported that some substances can regulate AMPK/Nrf2 pathway against liver injury[45,47].

Some reports have shown that chronic alcohol can lead to large amounts of lipid deposition in liver by disrupting lipid metabolism process, eventually causing steatosis[39]. In our work, TC and TG contents in serum were obviously increased, and HDL-C content was decreased by alcohol, which were in accordance with the previous report[48]. The Oil red O staining also confirmed the above results. However, lipid metabolism disorder was significantly reversed by ES1 treatment. To further explore the underlying mechanism of ES1 against steatosis, AMPK signaling pathway was also tested. Steatosis caused by long-term alcohol intervention may be directly related to inhibiting AMPK pathway[11]. Herath et al.[49] and Fang et al.[39] have found that hepatic AMPK and PPAR expressions fed with alcohol for a long time was significantly reduced and SREBP-1c expression was enhanced. Interestingly, ES1 could increase AMPKα phosphorylation and PPARα expression, decrease SREBP-1, SCD and FAS expressions. Similar studies also have reported that some substances can regulate AMPK pathway against hepatosteatosis in ALD mice[6]. These results manifested that ES1 could control AMPK pathway to up-regulate PPARα expression and down-regulate SREBP-1 for inhibiting SCD and FAS against lipid metabolism disorders in ALD mice, thereby preventing liver injury.

Substantial evidence have suggest that plays an important role in the occurrence and development of ALD[26]. Some reports have indicated that alcohol may directly and/or indirectly lead to dysbiosis of gut microbiota for increasing endotoxins, thereby injuring gut barrier, which caused harmful substances into liver by "gut-liver axis" for liver injury[50]. Natural polysaccharides play an important role in regulating gut microbiota against ALD[26,51]. In our work, ES1 could obviously improve the gut microbiota disorder in ALD mice. Meantime, correlation analysis between relevant biochemical indexes (AST, ALT, TC, TG, ROS, CAT, GSH-Px and SOD) and gut microbiota showed that ES1-mediated gut microbiota was closely related to the occurrence and development of ALD. By series of data analysis, ES1 increased the relative abundances of *Ligilactobacillus* and *Akkermansia*, and reduced the relative abundances of *Enterococcus*, *Romboutsia*, *Allobaculum*, Coriobacteriaceae_UCG-002, *Dubosiella*

and *Faecalibaculum*. *Ligilactobacillus* has been regarded as bacteria with potential anti-inflammatory effect, and Xu et al.[52] have found that *Gastrodia elata* polysaccharides can up-regulate the relative abundance of *Ligilactobacillus* against inflammatory bowel disease. *Akkermansia*, a recognized probiotic, plays an important role in the treatment of many diseases[53]. Although ES1 could increase the abundance of *Akkermansia*, it was not associated with related of indicators ALD, which might be because that *Akkermansia* regulate other microbes to play a role. Some reports have showed that Coriobacteriaceae_UCG-002 and *Faecalibaculum* are positively correlated with serum lipid levels in the occurrence and development of non-alcoholic fatty liver[54], which was consistent with our analysis. Yamamoto et al.[55] and Wang et al.[56] have found that *Romboutsia* and *Allobaculum* were harmful genera for accelerating the occurrence and development of obesity. Furthermore, *Enterococcus* and *Dubosiella* have been deemed to be a marker for facilitating inflammatory against intestinal barrier[20,57]. These results showed that ES1 had the ability to increase probiotics and reduce harmful bacteria in ALD mice. Meantime, we also tested colonic tight junction proteins and colonic histopathology, finding that ES1 could repair alcohol-induced dysfunction of intestinal barrier.

Some reports have showed some substances can produce short-chain fatty acids by regulating beneficial bacteria in gut microbiota for activating AMPK/Nrf2 pathway against liver injury[45]. Our results displayed that ES1 could increase the abundance of *Ligilactobacillus* and *Akkermansia* in feces of ALD mice. Interestingly, previous literatures have indicated both *Ligilactobacillus* and *Akkermansia* could produce large amounts of short chain fatty acids (SCFAs)[58-62]. Therefore, combining the relevant literature and our results, we speculated that the main way of ES1 alleviating alcohol-induced liver injury was that ES1 increased the relative abundances of *Ligilactobacillus* and *Akkermansia* producing SCFAs, thereby activating AMPK/Nrf2 pathway against oxidative stress and lipometabolic disturbance. Although our work has many significant findings, there are still some limitations in some respects. In our work, the relationship among the gut microbe, AMPK/Nrf2 pathway, ALD and ES1 still need further verification. Firstly, further work will be needed to investigate changes in SCFAs. Secondly, it is necessary to test effects of fecal transplantation on AMPK/Nrf2 and SCFAs. Finally, the relationship among the gut microbe, AMPK/Nrf2 pathway, ALD and ES1 is still verified by *in vitro* experiments.

5. Conclusion

In our work, ES1 from the fruiting bodies of *L. sulphureus*, obtained by a DEAE Seplife FF chromatographic column and a Sephacryl S-400HR column, was made up of *α*-*D*-Man*p*-(1→, →2,6)-*α*-*D*-Gal*p*-(1→, →6)-*α*-*D*-Gal*p*-(1→, →3)-*α*-*L*-Fuc*p*-(1→, and *α*-*D*-Glc*p*-(1→ with 25.79 kDa, as well as its structure was inferred. Meantime, we also explored the hepatoprotective activity of ES1 and its underlying mechanism in ALD mice. Combining the relevant literature and our results, we speculated that the main way of ES1 alleviating alcohol-induced liver injury was that ES1 increased the relative abundances of *Ligilactobacillus* and *Akkermansia* producing SCFAs, thereby activating AMPK/Nrf2 pathway against oxidative stress and lipometabolic disturbance (Fig. 10). Therefore, these data support the application of ES1 as a potential drug or functional food for treating ALD.

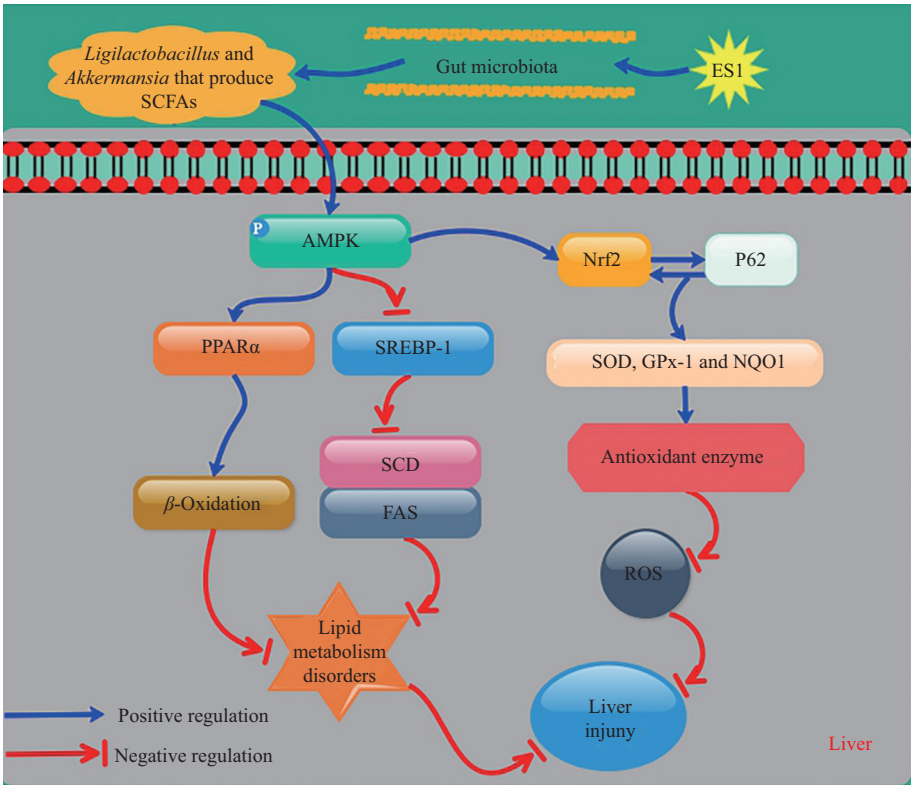

Fig. 10 Possible molecular mechanisms of ES1 against chronic ALD in mice.

Conflicts of interest

The authors declare that they have no known competing financial interests or personal relationships that could have appeared to influence the work reported in this paper.

Acknowledgments

This work was supported by grants from National Natural Science Foundation of China (82304113, 22107089 and 52271251), the Science and Technology Research Project of Henan Province (242102310526 and 232102310041), the Key project of Natural Science Foundation of Henan Province (242300421210), and the Doctoral Scientific Research Foundation of Xinxiang Medical University (XYBSKYZZ202123).

Appendix A. Supplementary data

Supplementary data associated with this article can be found, in the online version, at http://doi.org/10.26599/FSHW.2024.9250405.

References

[1] W.H. Jiang, H.K. Zhu, W.Q. Xu, et al., *Echinacea purpurea* polysaccharide prepared by fractional precipitation prevents alcoholic liver injury in mice by protecting the intestinal barrier and regulating liver-related pathways, Int. J. Biol. Macromol. 187 (2021) 143-156. https://doi.org/10.1016/j.ijbiomac.2021.07.095.

[2] J.G. Fan, Epidemiology of alcoholic and nonalcoholic fatty liver disease in China, J. Gastroen. Hepatol. 28 (2013) 11-17. https://doi.org/10.1111/jgh.12036.

[3] X.X. Jiang, Y.F. Zhou, Y. Zhang, et al., Hepatoprotective effect of pyrroloquinoline quinone against alcoholic liver injury through activating Nrf2-mediated antioxidant and inhibiting TLR4-mediated inflammation responses, Process Biochem. 92 (2020) 303-312. https://doi.org/10.1016/j.procbio.2020.01.023.

[4] K. Yang, X.F. Zhang, D. Liu, et al., Water extracts of *Pueraria thomsonii* Radix ameliorates alcoholic liver disease *via* PI3K/AKT and NOX4/ROS pathways, J. Funct. Foods 110 (2023) 105830. https://doi.org/10.1016/j.jff.2023.105830.

[5] A. Dogra, F. Li, Small-molecule chemical probes for the potential therapeutic targets in alcoholic liver diseases, Liver 7 (2023) 177-188. https://doi.org/10.1016/j.livres.2023.09.001.

[6] L. Qiu, R.B. Feng, Q.S. Wu, et al., Total saponins from *Panax japonicus* attenuate acute alcoholic liver oxidative stress and hepatosteatosis by p62-related Nrf2 pathway and AMPK-ACC/PPARα axis *in vivo* and *in vitro*, J. Ethnopharmacol. 317 (2023) 116785. https://doi.org/10.1016/j.jep.2023.116785.

[7] R.F. Cheng, M.K. Sun, Q.R. Hu, et al., *Hovenia acerba* Lindl. peduncles and seeds extracts ameliorate alcoholic liver injury by activating the Nrf2/HO-1 signalling pathway in LO2 cells and mice, Food Biosci. 51 (2023) 102224. https://doi.org/10.1016/j.fbio.2022.102224.

[8] H. Zhao, S. Li, J. Zhang, et al., The antihyperlipidemic activities of enzymatic and acidic intracellular polysaccharides by *Termitomyces albuminosus*, Carbohydr. Polym. 151 (2016) 1227-1234. https://doi.org/10.1016/j.carbpol.2016.06.058.

[9] A. Nagappan, D.Y. Jung, J.H. Kim, et al., Gomisin N alleviates ethanol-induced liver injury through ameliorating lipid metabolism and oxidative stress, Int. J. Mol. Sci. 19 (2018) 2601. https://doi.org/10.3390/ijms19092601.

[10] Q.X. Lu, Y.Y. Shu, L. Wang, et al., The protective effect of *Veronica ciliata* Fisch. extracts on relieving oxidative stress-induced liver injury *via* activating AMPK/p62/Nrf2 pathway, J. Ethnopharmacol. 270 (2021) 113775. https://doi.org/10.1016/j.jep.2021.113775.

[11] J. Lu, Y. Zhang, Y.Z. Wang, et al., Caffeic acid dimethyl ether alleviates alcohol-induced hepatic steatosis *via* microRNA-378b-mediated CaMKK2-AMPK pathway, Bioengineered 13 (2022) 11122-11136. https://doi.org/10.1080/21655979.2022.2060586.

[12] M.J. Kim, M.O. Sim, H.I. Lee, et al., Dietary umbelliferone attenuates alcohol-induced fatty liver *via* regulation of PPARα and SREBP-1c in rats, Alcohol 48 (2014) 707-715. https://doi.org/10.1016/j.alcohol.2014.08.008.

[13] A. Tripathi, J. Debelius, D.A. Brenner, et al., The gut-liver axis and the intersection with the microbiome, Nat. Rev. Gastro. Hepat. 15 (2018) 397-411. https://doi.org/10.1038/s41575-018-0011-z.

[14] S.B. Jasmohan, Alcohol, liver disease and the gut microbiota, Nat. Rev. Gastro. Hepat. 16 (2019) 235-246. https://doi.org/10.1038/s41575-018-0099-1.

[15] G. Ferrere, L. Wrzosek, F. Cailleux, et al., Fecal microbiota manipulation prevents dysbiosis and alcohol-induced liver injury in mice, J. Hepatol. 66 (2017) 806-815. https://doi.org/10.1016/j.jhep.2016.11.008.

[16] S.A.M. Albhaisi, J.S. Bajaj, A.J. Sanyal, Role of gut microbiota in liver disease, Am. J. Physiol-Gastr. L. 318 (2020) G84-G98. https://doi.org/10.1152/ajpgi.00118.2019.

[17] M. Llopis, A.M. Cassard, L. Wrzosek, et al., Intestinal microbiota contributes to individual susceptibility to alcoholic liver disease, Gut 65 (2016) 830-839. https://doi.org/10.1136/gutjnl-2015-310585.

[18] C.A. Philips, A. Pande, S.M. Shasthry, et al., Healthy donor fecal microbiota transplantation in steroid-ineligible severe alcoholic hepatitis: a pilot study, Clin. Gastroenterol. H. 15 (2017) 600-602. https://doi.org/10.1016/j.cgh.2016.10.029.

[19] H.J. Zhao, H.P. Li, Q.Q. Lai, et al., Antioxidant and hepatoprotective activities of modified polysaccharides from *Coprinus comatus* in mice with alcohol-induced liver injury, Int. J. Biol. Macromol. 127 (2019) 476-485. https://doi.org/10.1016/j.ijbiomac.2019.01.067.

[20] H.J. Zhao, M. Li, L. Liu, et al., *Cordyceps militaris* polysaccharide alleviates diabetic symptoms by regulating gut microbiota against TLR4/NF-κB pathway, Int. J. Biol. Macromol. 230 (2023) 123241. https://doi.org/10.1016/j.ijbiomac.2023.123241.

[21] C. Jen, M.K. Lu, M.N. Lai, et al., Sulfated polysaccharides of *Laetiporus sulphureus* fruiting bodies exhibit anti-breast cancer activity through cell cycle arrest, apoptosis induction, and inhibiting cell migration, J. Ethnopharmacol. 321 (2024) 117546. https://doi.org/10.1016/j.jep.2023.117546.

[22] M.K. Lu, C. Jen, C.H. Chao, et al., SPS, a sulfated galactoglucan of *Laetiporus sulphureus*, exhibited anti-inflammatory activities, Int. J. Biol. Macromol. 226 (2023) 1236-1247. https://doi.org/10.1016/j.ijbiomac.2022.11.237.

[23] H.J. Zhao, Y.F. Lan, H. Liu, et al., Antioxidant and hepatoprotective activities of polysaccharides from spent mushroom substrates (*Laetiporus sulphureus*) in acute alcohol-induced mice, Oxid. Med. Cell. Longev. 2017 (2017) 5863523. https://doi.org/10.1155/2017/5863523.

[24] A.Q. Zhang, J.Y. Deng, S.Y. Yu, et al., Purification and structural elucidation of a water-soluble polysaccharide from the fruiting bodies of the *Grifola frondose*, Int. J. Biol. Macromol. 115 (2018) 221-226. https://doi.org/10.1016/j.ijbiomac.2018.04.061.

[25] Y.X. Wang, T. Zhang, Y. Xin, et al., Comprehensive evaluation of alkali-extracted polysaccharides from *Agrocybe cylindracea*: comparison on structural characterization, Carbohydr. Polym. 255 (2021) 117502. https://doi.org/10.1016/j.carbpol.2020.117502.

[26] W. Cao, J.Q. Wu, X.Y. Zhao, et al., Structural elucidation of an active polysaccharide from *Radix Puerariae lobatae* and its protection against acute alcoholic liver disease, Carbohydr. Polym. 325 (2024) 121565. https://doi.org/10.1016/j.carbpol.2023.121565.

[27] H. Zhang, C.C. Li, J. Ding, et al., Structural features and emulsifying stability of a highly branched arabinogalactan from immature peach (*Prunus persica*) exudates, Food Hydrocoll. 104 (2020) 105721. https://doi.org/10.1016/j.foodhyd.2020.105721.

[28] B.H. Wang, J.J. Cao, B. Zhang, et al., Structural characterization, physicochemical properties and α-glucosidase inhibitory activity of polysaccharide from the fruits of wax apple, Carbohydr. Polym. 211 (2019) 227-236. https://doi.org/10.1016/j.carbpol.2019.02.006.

[29] L. Wang, H.M. Liu, A.J. Xie, et al., Chinese quince (*Chaenomeles sinensis*) seed gum: structural characterization, Food Hydrocolloid. 75 (2018) 237-245. https://doi.org/10.1016/j.foodhyd.2017.08.001.

[30] S.M. Sanches Lopes, G. Krausova, J.W. Pedroza Carneiro, et al., A new natural source for obtainment of inulin and fructo-oligosaccharides from industrial waste of *Stevia rebaudiana* Bertoni, Food Chem. 225 (2017) 154-161. https://doi.org/10.1016/j.foodchem.2016.12.100.

[31] Z. Liang, Z. Yin, X. Liu, et al., A glucomannogalactan from *Pleurotus geesteranus*: structural characterization, chain conformation and immunological effect, Carbohydr. Polym. 287 (2022) 119346. https://doi.org/10.1016/j.carbpol.2022.119346.

[32] L. Yu, S.Q. Xu, C. Deng, et al., Preparation and partial structural characterization of the exopolysaccharide from *Bacillus mucilaginosus* SM-01, Carbohydr. Polym. 146 (2016) 217-223. https://doi.org/10.1016/j.carbpol.2016.03.038.

[33] J.M. Schwartz, J.F. Reinus, Prevalence and natural history of alcoholic liver disease, Clin. Liver Dis. 16 (2012) 659-666. https://doi.org/10.1016/j.cld.2012.08.001.

[34] W.W. Chao, S.J. Chen, H.C. Peng, et al., Antioxidant activity of *Graptopetalum paraguayense* E. Walther leaf extract counteracts oxidative stress induced by ethanol and carbon tetrachloride Co-induced hepatotoxicity in rats, Antioxidants 8 (2019) 251. https://doi.org/10.3390/antiox8080251.

[35] Y.C. Fu, Z.Y. Zeng, S.W. Feng, et al., JBB attenuates acute and chronic alcoholic liver injury by regulating the NFκB, KEAP1, and HIF1 pathways, J. Funct. Foods 109 (2023) 105782. https://doi.org/10.1016/j.jff.2023.105782.

[36] X. Zhou, Q.F. Deng, H.G. Chen, et al., Characterizations and hepatoprotective effect of polysaccharides from *Mori Fructus* in rats with alcoholic-induced liver injury, Int. J. Biol. Macromol. 102 (2017) 60-67. https://doi.org/10.1016/j.ijbiomac.2017.03.083.

[37] Z. Ma, Y. Zhang, Q. Li, et al., Resveratrol improves alcoholic fatty liver disease by downregulating HIF-1α expression and mitochondrial ROS production, PLoS One 12 (2017) e183426. https://doi.org/10.1371/journal.pone.0183426.

[38] F. Wang, J.C. Liu, R.J. Zhou, et al., Apigenin protects against alcohol-induced liver injury in mice by regulating hepatic CYP2E1-mediated oxidative stress and PPARα-mediated lipogenic gene expression, Chem-Biol. Interact. 275 (2017) 171-177. https://doi.org/10.1016/j.cbi.2017.08.006.

[39] C.Q. Fang, J.Z. Zhang, J.J. Han, et al., Tiaogan Jiejiu Tongluo Formula attenuated alcohol-induced chronic liver injury by regulating lipid metabolism in rats, J. Ethnopharmacol. 317 (2023) 116838. https://doi.org/10.1016/j.jep.2023.116838.

[40] H.C. Wang, J.J. Yan, K. Wang, et al., The gut-liver axis perspective: exploring the protective potential of polysaccharides from *Cistanche deserticola* against alcoholic liver disease, Int. J. Biol. Macromol. 256 (2024) 128394. https://doi.org/10.1016/j.ijbiomac.2023.128394.

[41] Y. Han, S. Nan, J. Fan, et al., *Inonotus obliquus* polysaccharides protect against Alzheimer's disease by regulating Nrf2 signaling and exerting antioxidative and antiapoptotic effects, Int. J. Biol. Macromol. 131 (2019) 769-778. https://doi.org/10.1016/j.ijbiomac.2019.03.033.

[42] H.Q. Gou, X. Chen, X.M. Zhu, et al., Sequestered SQSTM1/p62 crosstalk with Keap1/NRF2 axis in hPDLCs promotes oxidative stress injury induced by periodontitis, Free Radical Bio. Med. 190 (2022) 62-74. https://doi.org/10.1016/j.freeradbiomed.2022.08.001.

[43] X.H. Su, W.Y. Guo, B. Yuan, et al., Artesunate attenuates bone erosion in rheumatoid arthritis by suppressing reactive oxygen species *via* activating p62/Nrf2 signaling, Biomed. Pharmacother. 137 (2021) 111382. https://doi.org/10.1016/j.biopha.2021.111382.

[44] C. Mo, L. Wang, J. Zhang, et al., The crosstalk between Nrf2 and AMPK signal pathways is important for the anti-inflammatory effect of berberine in LPS-stimulated macrophages and endotoxin-shocked mice, Antioxid. Redox Signal. 20 (2014) 574-588. https://doi.org/:10.1089/ars.2012.5116.

[45] W. Peng, C.X. He. R.L. Li, et al., *Zanthoxylum bungeanum* amides ameliorates nonalcoholic fatty liver *via* regulating gut microbiota and activating AMPK/Nrf2 signaling, J. Ethnopharmacol. 318 (2024) 116848. https://doi.org/10.1016/j.jep.2023.116848.

[46] P. Jiang, L.J. Ren, L. Zhi, et al., Negative regulation of AMPK signaling by high glucose *via* E3 ubiquitin ligase MG53, Mol. Cell 81 (2021) 629-637. https://doi.org/10.1016/j.molcel.2020.12.008.

[47] X.Q. Ding, T.Y. Jian, J.W. Li, et al., Chicoric acid ameliorates nonalcoholic fatty liver disease *via* the AMPK/Nrf2/NFκB signaling pathway and restores gut microbiota in high-fat-diet-fed mice, Oxid. Med. Cell. Longev. 2020 (2020) 9734560. https://doi.org/10.1155/2020/9734560.

[48] Y.G. Liu, R.L. Chen, L.Z. Li, et al., The triterpenoids-enriched extracts from *Antrodia cinnamomea* mycelia attenuate alcohol-induced chronic liver injury *via* suppression lipid accumulation in C57BL/6 mice, Food Sci. Hum. Wellness 10 (2021) 497-507. https://doi.org/10.1016/j.fshw.2021.04.012.

[49] K.H.I.N.M. Herath, J. Cho, A. Kim, et al., Phenolic acid and flavonoid-rich fraction of *Sasa quelpaertensis* Nakai leaves prevent alcohol induced fatty liver through AMPK activation, J. Ethnopharmacol. 224 (2018) 335-348. https://doi.org/10.1016/j.jep.2018.06.008.

[50] S. Patel, R. Behara, G.R. Swanson, et al., Alcohol and the intestine, Biomolecules 5 (2015) 2573-2588. https://doi.org/10.3390/biom5042573.

[51] X.L. Song, W.J. Cui, F.Y. Meng, et al., Glucopyranose from *Pleurotus geesteranus* prevent alcoholic liver diseases by regulating pathways and gut microbiota, Food Funct. 13 (2022) 2441-2455. https://doi.org/10.1039/d1fo03486c.

[52] D. Xu, Q.Y. Wu, W.Y. Liu, et al., Therapeutic efficacy and underlying mechanisms of *Gastrodia elata* polysaccharides on dextran sulfate sodium-induced inflammatory bowel disease in mice: modulation of the gut microbiota and improvement of metabolic disorders, Int. J. Biol. Macromol. 248 (2023) 125919. https://doi.org/10.1016/j.ijbiomac.2023.125919.

[53] X. Wu, W.X. Xuan, X.P. Yang, et al., Ficolin A knockout alleviates sepsis-induced severe lung injury in mice by restoring gut *Akkermansia* to inhibit S100A4/STAT3 pathway, Int. J. Biol. Macromol. 121 (2023) 110548. https://doi.org/10.1016/j.intimp.2023.110548.

[54] H. Mu, Q. Zhou, R. Yang, et al., Naringin attenuates high fat diet induced non-alcoholic fatty liver disease and gut bacterial dysbiosis in mice, Front. Microbiol. 11 (2020) 585066. https://doi.org/10.3389/fmicb.2020.585066.

[55] M. Yamamoto, H. Ogura, T. Kuda, et al., Effects of roasted burdock root tea, drink, and the residue on caecal microbiota of mice fed low-dietary fibre diet, Food Chem. Adv. 3 (2023) 100376. https://doi.org/10.1016/j.focha.2023.100376.

[56] Y. Wang, N. Ablimit, Y.P. Zhang, et al, Novel *β*-mannanase/GLP-1 fusion peptide high effectively ameliorates obesity in a mouse model by modifying balance of gut microbiota, Int. J. Biol. Macromol. 191 (2021) 753-763. https://doi.org/10.1016/j.ijbiomac.2021.09.150.

[57] K.L. Sheng, G.H. Zhang, M. Sun, et al., Grape seed proanthocyanidin extract ameliorates dextran sulfate sodium-induced colitis through intestinal barrier improvement, oxidative stress reduction, and inflammatory cytokines and gut microbiota modulation, Food Funct. 11 (2020) 7817-7829. https://doi.org/10.1039/d0fo01418d.

[58] M.Y. Yuan, L.L. Chang, P. Gao, et al., Synbiotics containing sea buckthorn polysaccharides ameliorate DSS-induced colitis in mice *via* regulating Th17/Treg homeostasis through intestinal microbiota and their production of BA metabolites and SCFAs, Int. J. Biol. Macromol. 276 (2024) 133794. https://doi.org/10.1016/j.ijbiomac.2024.133794.

[59] J.Y. Ge, Z.N. Zhou, Y. Zhou, et al., 2'-Fucosyllactose promotes the enrichment of *Akkermansia muciniphila* and the production of short-chain fatty acids *in vitro* and *in vivo*, Food Biosci. 61 (2024) 104785. https://doi.org/10.1016/j.fbio.2024.104785.

[60] M.SA. Palmnäs-Bédard, G. Costabile, C. Vetrani, et al., The human gut microbiota and glucose metabolism: a scoping review of key bacteria and the potential role of SCFAs, Am. J. Clin. Nutr. 116 (2022) 862-874. https://doi.org/10.1093/ajcn/nqac217.

[61] O.J. Sobrino1, C. Alba, R. Arroyo, et al., Replacement of metaphylactic antimicrobial therapy by oral administration of *Ligilactobacillus salivarius* MP100 in a pig farm, Front. Veter. Sci. 8 (2021) 666887. https://doi.org/10.3389/fvets.2021.666887.

[62] S.Y. Zhou, H.X. Zhou, J. Qian, et al., Compound prebiotics as prophylactic and adjunctive treatments ameliorate DSS-induced colitis through gut microbiota modulation effects, Int. J. Biol. Macromol. 270 (2024) 132362. https://doi.org/10.1016/j.ijbiomac.2024.132362.